Received: 27 February 2024 | Revised: 9 April 2024 | Accepted: 11 April 2024

DOI: 10.1002/aoc.7499

RESEARCH ARTICLE

Applied Organometallic Chemistry WILEY

An experimental and computational studies, evaluating the in vitro antidiabetic and antioxidant activity, in silico prediction ADMET properties of 5-chloro-1H-benzimidazole and its newly synthesized silver(I) complex

Ceyhun Kucuk[1] | **Sibel Celik**[2] | **Senay Yurdakul**[3] | **Ebru Coteli**[2]

[1]Ahmet Erdogan Vocational School of Health Services, Zonguldak Bulent Ecevit University, Zonguldak, Turkey

[2]Vocational School of Health Services, Kırsehir Ahi Evran University, Kırşehir, Turkey

[3]Department of Physics, Faculty of Science, Gazi University, Ankara, Turkey

Correspondence
Ceyhun Kucuk, Ahmet Erdogan Vocational School of Health Services, Zonguldak Bulent Ecevit University, Zonguldak, Turkey.
Email: ceyhun.kucuk@beun.edu.tr

In this research, a new Ag(I) complex, namely, [Ag(5-chloro-1H-benzimidazole)$_2$(NO_3)], has been synthesized using the benzimidazole-based ligand 5-chloro-1H-benzimidazole (5ClBZ). Ag(I) complexes were characterized by elemental analysis, UV-Vis, FT-IR, and ^{1}H NMR spectroscopy, and DFT analysis was used. The free ligand and its Ag(I) complexes were tried for their biochemical properties, including antioxidant and antidiabetic properties. To study the molecular structures of the title compounds, in silico ADME/Tox research was performed on the newly made complex and free ligand. The empirical guidelines relating to ADME were utilized to conduct molecular docking simulations and in-depth drug-likeness profiling. This was carried out to validate the conclusions and identify exact binding interactions. Based on the study's findings, it has been determined that these new compounds have significant potential as powerful therapeutic agents for controlling antioxidant and antidiabetic activities.

KEYWORDS

5-chloro-1H-benzimidazole, ADME, antidiabetic, antioxidant, DFT, molecular docking

1 | INTRODUCTION

A species of bicyclic aromatic chemical compound, benzimidazole, is the benzo derivative of imidazole. It consists of five-membered imidazole fused to a six-membered benzene ring at the four and five locations of the imidazole ring.[1] It is a structure with various biologically active properties, such as analgesics.[2,3] antiparasitic,[4] antifungals,[5] anticoagulants, anti-inflammatory agents,[6] antihypertensives,[7] antihistaminic,[8] antimalarial,[9] antitubercular,[10] anti-HIV,[11] antimicrobial,[12] antiprotozoal,[13] andantiviral,[14] and is also used as a drug-active ingredient in the field of pharmacology. Various benzimidazole-based drugs, such as prazole, rabeprazole, and timoprazole, are widely used as proton pump inhibitors in the treatment of ulcers and gastritis.[15] Benzimidazole is a corrosion inhibitor used in metals and alloys. Transition metal salt complexes with benzimidazole derivatives have been intensively investigated as biological molecular models.[16]

Argentophilic interactions between d^{10} metal ions, especially silver (I) ions, play an important role in building fascinating structures and influencing the properties of structural architectures.[17] The noble metal Ag ions

have been used as a permanent pathogenic organism inhibitor.[18] The Ag ions have powerful inhibitory effects and are called permanent inhibitors against pathogenic organisms.

In recent years, the use of metal drugs in the medical sciences has attracted attention.[19–22] Metal complexes containing some bioactive ligands are sometimes more effective than free ligands in biological and drug applications.[23–26] Metal complexes have numerous biological effects, including antidiabetic, anti-cancer, antibacterial, and anti-inflammatory measures, among others.[27,28] People are of the opinion that metal combinations can be utilized in metallotherapy, an innovative diabetes treatment. Numerous investigations to date have demonstrated that transition metal complexes containing various ligands exhibit insulin-like activity and α-amylase inhibition activity.[29] Hydrolytic enzymes, including intestinal α-glucosidases and pancreatic α-amylase, break down carbs into glucose in the body.[30] It is stated in the literature that inhibiting these two enzymes results in a decrease in the use of carbohydrates in the diet and also suppresses postprandial glycemia. These side effects may be caused by excessive inhibition of pancreatic α-amylase, which leads to abnormal bacterial fermentation of undigested carbohydrates in the colon.[19] In addition, a large number of transition metal complexes have been reported to exhibit effective antioxidant resistance over the past few years.[31] In most diseases, the oxidative stress imbalance between free radical generation and reactive metabolites is the main problem. Chronic diseases are influenced by oxidative stress, cytotoxicity, and inflammation. Damaged free radicals and synchronized loss of antioxidant defense mechanisms can delicately disturb cellular organelles and enzymes, causing lipid peroxidation and insulin resistance, which can lead to diabetes problems.[32]

Further, scientists have perceived that coordination chemistry research has been expanded by utilizing DFT-based studies like MEP, HOMO-LUMO, and Fukui function parameters as evidence for complex areas of electrophilicity/nucleophilicity and reactivity activities. Spectroscopic methods and density functional theory (DFT) have recently been used to identify the structures of a range of organic molecules.[33,34] These compounds have been synthesized and characterized by spectroscopic techniques (IR, UV-vis, and 1H–NMR) in order to study their antidiabetic and antioxidant activities. The aim of this paper is to synthesize a new compound and investigate their antioxidant capacities and radical scavenging activities for summarizing their biochemical properties. The antidiabetic and antioxidant properties of the compounds have been studied to demonstrate their possibility of acting against oxidative stress-induced diseases. Complex structures containing silver ion have been used for many purposes, like surgery, wound care products, antioxidants, and antidiabetic.[35] These synthesized silver complex are tested to assess their antioxidant activity by detecting the 2,2-diphenyl-1-picrylhydrazyl (DPPH) and 2,2′-azino-bis3-ethylbenzthiazoline-6-sulfonic acid (ABTS) scavenging activities and antidiabetic (alpha amylase enzyme inhibition) activities, which demonstrated that Ag(I) metal complex possess potent antioxidant properties. In addition, the ADMET study was accomplished to predict the pharmacokinetic, toxicity, and physicochemical properties of the title compounds.

2 | MATERIAL AND METHODS

2.1 | Computational methods

All calculations regarding DFT were calculated using the Gaussian 09 package program, and the visualizations required for these calculations were created in the Gauss Viev 5.0.9 program.[36,37] The 5ClBZ molecule was optimized at the B3LYP/6-311++G(d,p) level.[38–40] The [Ag $(5ClBZ)_2(NO_3)$] complex was also optimized by using a combination of the 6-311++G(d,p) basis set for light atoms (C, H, O, and Cl) and the LanL2DZ basis set for the heavy atom (Ag) in the same method and functional.[41] The vibrational modes of the synthesized Ag(I) complex of the 5ClBZ molecule were assigned with the VEDA program according to the total energy distribution (TED).[42] Frequency values for the [Ag $(5ClBZ)_2(NO_3)$] complex were calculated using the B3LYP/6-311++G(d,p) basis set and the LanL2DZ basis set for optimized structure. The HOMO-LUMO energies, MEP map, and Fukui functions were calculated for the 5ClBZ molecule in the B3LYP/6-311++G(d,p) basis set.[40] Also, calculations for the $[Ag(5ClBZ)_2(NO_3)]$ complex were performed using the same method and a functional with a combination of the 6-311++G(d,p) (for C, H, N, and Cl atoms) and LanL2DZ (Ag atom) basis sets.[41] The visual map of the dual descriptors calculated from the Fukui functions was created using the Multiwfn package program.[43] The ^1H NMR chemical shift values for the 5CLBZ molecule and the $[Ag(5ClBZ)_2(NO_3)]$ complex are calculated using DFT/B3LYP/6-311 + G(2d,p)[44] and DFT/B3LYP/6-311 + G(2d,p) + LanL2DZ[45] at levels of theory, respectively, in the IEFPCM/DMSO model with the GIAO method.

The molecular docking of the chemical ligand-protein binding site was performed using Autodock 2.2.6 software.[46] The primary repository for PDB structures

utilized as target proteins is RCSB. The receptors for the antioxidant enzyme (PDB ID: 3NM8) and the pancreatic enzyme α-amylase (PDB ID: 2QV4) were identified using the RCSB Protein Data Bank.[47] The nonbonding interactions of the active site of the receptor pocket are explored using Discover Studio Visualizer 21. The online tools SwissADME[48] and PreADMET were used to predict the ADME profiles of compounds.[49] The organ toxicities and toxicological end points of the free ligand and its Ag(I) complex were estimated using the Protox-II website.[50]

2.2 | Experimental methods

2.2.1 | Syenthesis

5-Chlorobenzimidazole (96% purity) (CAS Number: 4887-82-5) and silver nitrate (99.5% purity) (CAS Number: 7761-88-8) molecules were supplied from Sigma Aldric Chemical Company. While the silver nitrate complex of the 5CIBZ molecule was formed, no further purification process was performed for these molecules. First of all, a 2 mmol (0.3052 g) solution of 5ClBZ molecules in 20 mL of ethanol (99,8% purity) at 50°C and 1 mmol (0.1698 g) silver nitrate solutions in 10 mL of ethanol were prepared. Then, the prepared silver nitrate solution was added dropwise to the 5CLBZ solution and stirred at 50°C for 3 h, preventing evaporation. As a result of this process, a white precipitate was obtained. As a result of the elemental analysis of the synthesized complex, the ligand/metal ratio of the chemical produced is 2:1. Experimental and theoretical percentage ratios for C, H, and N atoms in complex are as follows: $[Ag(C_7H_5ClN_2)_2(NO_3)]$ ($5ClBZ = C_7H_5ClN_2$), CHN Exp: C: 36.40%, H: 2.57%, N: 14.30% and Calc: C: 35.39%, H: 2.12%, N: 14.74%. The synthesis scheme of the $[Ag(5ClBZ)_2(NO_3)]$ complex is presented in Figure 1. The yield of the synthesized compound was 78%.

2.2.2 | Spectral analyses

Far-IR spectra were recorded in the region between 500 and 100 cm^{-1} using Bruker 66/S spectrometers. Also, FT-TIR spectra were recorded in the regions of 4000–500 cm^{-1} with the Bruker Vertekx 80 FT-IR. A Bruker 400MHZ AV model spectrometer was used to record the ^1H NMR spectrum. The spectra of both the free ligand and its synthesized silver nitrate complex were recorded in a DMSO solution. UV-Vis spectra for the title molecule and the synthesized complex were recorded with an Agilent HP 8453 spectrophotometer for ethanol solution in the range of 190–1100 nm.

2.2.3 | In vitro determination of antidiabetic activity

α-Amylase enzyme inhibition

The activity of α-amylase, a carbohydrate digestion enzyme, was determined in the presence and absence of the 5CIBZ molecule and the $[Ag(5ClBZ)_2(NO_3)]$ complex.[51] To determine the enzyme activity, 0.5 mL of starch and 0.5 mL of enzyme mixture were kept at 25°C for 20 min. 1 mL of DNS (3,5-dinitrosalicylic acid) solution was added to the samples, and the samples were boiled for 5 min; 7.5 mL of distilled water was added to the samples cooled in tap water. Absorbance was measured at $\lambda = 540$ nm. A control tube was used by substituting 0.5 mL of the buffer instead of the enzyme. To examine whether the extracts have an inhibitory effect on the α-amylase enzyme, 0.5 mL of extract at varying concentrations (25, 50, and 100 μg/mL) and 0.5 mL of enzyme were incubated at 37°C for 15 min. Then, 0.5 mL of starch was added to the medium, and the experiment was continued as stated above with the addition of DNS and boiling. A sample blank was run for each sample. When preparing the sample blanks, the same experimental procedure was

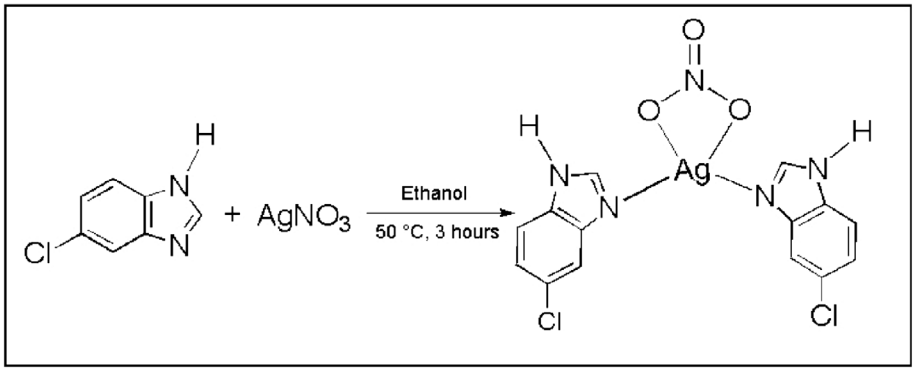

FIGURE 1 Synthesis scheme of the $[Ag(5ClBZ)_2(NO_3)]$ complex.

applied, replacing the enzyme with buffer. Acarbose standard material was used to compare the results of the samples. The α-amylase enzyme inhibition values of the samples or acarbose were calculated according to the formula below.

$$\%\text{Inhibition} = \frac{(\text{Absorbance amylase} - \text{Absorbance Extract/acarbose})}{\text{Absorbance amylase}} \times 100 \quad (1)$$

Absorbance amylase: The absorbance of the tube is considered 100% active; Absorbance extract: Sample absorbance − sample blank absorbance.

2.2.4 | In vitro determination of antioxidant activity

DPPH• (2,2-difenil-1-pikrilhidrazil) radical scavenging activity

The free radical scavenging activities of the 5CIBZ molecule and the $[Ag(5ClBZ)_2(NO_3)]$ complex were determined using the DPPH• radical.[52] Stock solutions of the 5CIBZ molecule and the $[Ag(5CIBZ)_2NO_3]$ complex at 1 mg/mL concentration in methanol were prepared. Samples were prepared from these solutions at three different concentrations (25, 50, and 100 μg/mL); 1 mL of these samples was taken, and 4 mL of a 0.1-mM DPPH solution was added. All samples were vortexed and allowed to stand in the dark for 30 min. The absorbance of the samples was measured at 517 nm in a spectrophotometer. The same experimental procedure was run for control tubes using methanol instead of extract. BHT was used as the standard substance to compare the results. The radical scavenging inhibition values of the samples were calculated with the following formula:

$$\%\text{Inhibition} = \frac{(\text{Absorbance control} - \text{Absorbance sample})}{\text{Absorbance control}} \times 100 \quad (2)$$

$ABTS^{\bullet+}$ [2,2′-Azino-bis (3-etilbenztiyazolin-6-sülfonik asit)] radical scavenging activity

The antioxidant activities of the 5CIBZ molecule and the $[Ag(5ClBZ)_2(NO_3)]$ complex were examined using another radical, the $ABTS^{\bullet+}$ cationic radical.[53] For this purpose, a 7-mM ABTS solution and a 2.45-mM $Na_2S_2O_8$ solution were prepared. These two prepared solutions were mixed in a ratio of 1:0.5. It was wrapped in aluminum foil and left for 16 h to allow the radicals to form. This radical solution was diluted with an 80% ethanol-water solution so that the absorbance at 734 nm was approximately 0.7. It was used in this form in the study. Solutions of the samples to be examined were prepared at three different concentrations: 25, 50, and 100 μg/mL; 50 μL of these samples were placed in test tubes; 2 mL of this radical solution was added to the samples and kept in a dark environment for 30 min. Then, their absorbance was measured at 734-nm wavelength in the spectrophotometer device. The same experimental procedure was applied by adding methanol instead of extract to the control tube. BHT was used as the standard substance in the $ABTS^{\bullet+}$ radical scavenging method. The same experimental procedure was repeated for the standards. The absorbance of all samples was measured, and the % inhibition values were calculated using the formula below.

$$\%\text{Inhibition} = [(\text{Absorbance control} - \text{Absorbance sample})/\text{Absorbance control}] \times 100 \quad (3)$$

2.2.5 | Statistical analysis

All analyses were conducted on three samples. The arithmetic means and standard deviations of the results were calculated using the Microsoft Office Excel program.

3 | RESULT AND DISCUSSION

3.1 | Geometric parameters

Geometric parameters for the free ligand and its Ag(I) complex are listed in Table S1, and optimized

structures are presented in Figures 2 and 3. The bond length and bond angle values of the 5ClBZ ligand were compared with the XRD data of 2-chlorobenzimidazole,[54] and those of the $[Ag(5ClBZ)_2(NO_3)]$ complex were compared with the XRD data of the (1H-Benzimidazole-5-carboxylic acid-κN3)(1H-benzimidazole-6-carboxylic acid-κN3)silver(I) perchlorate ($[Ag(C_8H_6N_2O_2)_2].ClO_4$) complex (see Table S1).[55]

While the N_1-C_9 and N_2-C_9 bond lengths were calculated as 1.375 and 1.305 Å for the free ligand, these bond lengths were calculated as 1.360 and 1.317 Å for the Ag(I) complex, Also, the N_{16}-C_{24} and N_{17}-C_{24} bond lengths of the $[Ag(5ClBZ)_2(NO_3)]$ complex were found to be 1.360 and 1.317 Å in the calculations. The N_1-C_3 and N_2-C_4 bond lengths of the imidazole ring of the 5ClBZ molecule were calculated as 1.384 and 1.387 Å, respectively. The bond lengths of N_1-C_3/N_{16}-C_{24} and N_2-C_4/N_{17}-C_{19} in the imidazole rings next to the $[Ag(5ClBZ)_2(NO_3)]$ complex were also calculated as 1.387 and 1.389 Å. The C_8-Cl_{14} bond length was found to be 1.763 for the free ligand, and the C_8-Cl_{14}/C_{23}-Cl_{29} bond lengths were found to be 1.759 Å in its Ag(I) complex. The N_2-Ag_{31} and N_{17}-Ag_{31} bond lengths of the complex structure were calculated as 2.238 Å, and the Ag_{31}-O_{33} and Ag_{31}-O_{34} bond lengths were calculated as 2.639 A. The O_{32}-N_{35}, O_{33}-N_{35}, and O_{34}-N_{35} bond lengths of the nitrate group were found to be 1.227, 1.273, and 1.273 Å, respectively.

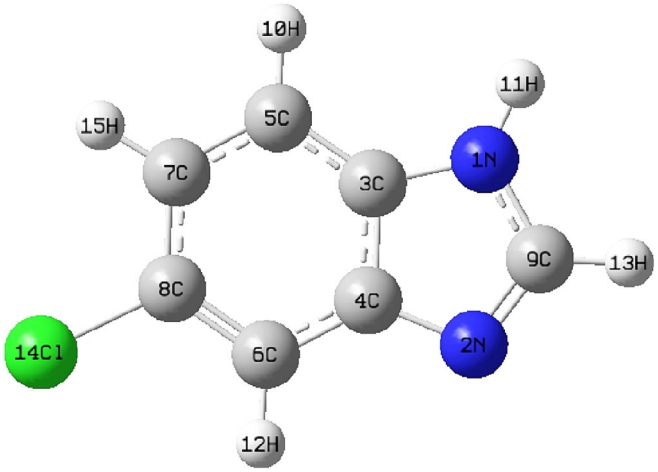

FIGURE 2 Optimized geometric structure of the 5ClBZ molecule.

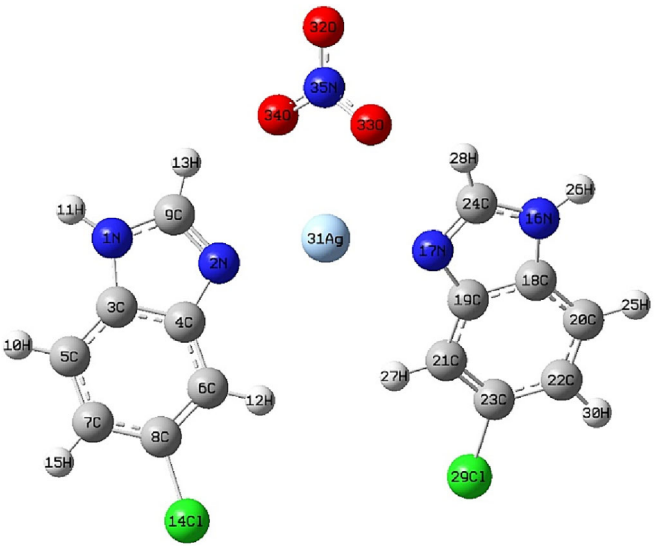

FIGURE 3 Optimized geometric structure of the $[Ag(5ClBZ)_2(NO_3)]$ complex.

While the C_3-N_1-C_9 and C_4-N_2-C_9 bond angles are calculated as 106.77° and 104.87° for the free ligand, these angles are 107.85° and 106.21°, respectively, in the complex structure. In addition, the bond angles of C_{18}-N_{16}-C_{24} and C_{19}-N_{17}-C_{24} for the title complex were found to be 107.85° and 106.21°. While the N_1-C_9-N_2 bond angle in the imidazole ring of the 5ClBZ molecule was calculated as 113.52, the N_1-C_9-N_2/N_{16}-C_{24}-N_{17} bond angles in the imidazole rings of the ligands in the structure of the $[Ag(5ClBZ)_2(NO_3)]$ complex were calculated as 111.99°. The N_2-Ag_{31}-N_{17} bond angle of the title complex was also calculated at 160.65°.

To compare the calculated bond length and bond angle values of the 5ClBZ molecule and the $[Ag(5ClBZ)_2(NO_3)]$ complex with the data of the 2-chlorobenzimidazole molecule and the $[Ag(C_8H_6N_2O_2)_2].ClO_4$ complex, respectively, correlation graphs were drawn (Figure S1), and R^2 values were calculated.

According to the correlation graph drawn to compare the bond length and bond angles of the 5ClBZ molecule with the 2-chlorobenzimidazole molecule, the R^2 values for bond lengths were calculated as 0.9833 and 0.9774 for bond angles. These results show that bond lengths and bond angles are compatible with each other because R^2 values are close to 1.

In the correlation graph prepared for the $[Ag(5ClBZ)_2(NO_3)]$ complex, the R^2 value obtained for bond lengths is 0.9985, and this value is 0.8745 for bond angles. The bond lengths of the cap complex are quite compatible with those of the $[Ag(C_8H_6N_2O_2)_2].ClO_4$ complex. Significant differences were determined between the C_4-N_2-Ag_{31}, C_9-N_2-Ag_{31}, C_{19}-N_{17}-Ag_{31}, and C_{24}-N_{17}-Ag_{31} bond angle values of the $[Ag(5ClBZ)_2(NO_3)]$ complex and the XRD data of the compared complex. Apart from these angle values, no significant difference was observed between the other angle values. The fact that the R^2 value is far from 1 is due to the discrepancy between these angle values.

3.2 | Vibrational analysis

Experimental frequency values were recorded for both the free ligand and the title complex and listed in Table 1. To ensure compatibility between experimental and theoretical frequency values, values below and above 1800 cm^{-1} were scaled with scale factors of 0.983[56] and 0.961,[57] respectively. Also, the experimental IR spectra for the 5ClBz molecule and the synthesized $[Ag(5ClBZ)_2(NO_3)]$ complex are presented in Figure S2.

3.2.1 | N-H stretching vibrations

The N-H stretching vibrations appear in the region of the IR spectrum in the range of 3500–3000 cm^{-1}.[58] These vibrational modes were not observed in the experimental IR spectra for the 5ClBZ molecule and the $[Ag(5ClBZ)_2(NO_3)]$ complex. The N-H stretching vibrations were calculated at 3094/3095 cm^{-1} for the title complex in the theoretical calculations. While this vibration mode is observed at 3600 cm^{-1} in the FT-IR spectrum of the benzimidazole molecule, the theoretical value is calculated at 3513 cm^{-1}.[59]

3.2.2 | C-H stretching vibrations

The C-H stretching vibrations of heterocyclic aromatic compounds are generally observed in the region of 3100–3000 cm^{-1}.[60] This stretching vibration was determined at 3038 (w) cm^{-1} for the free ligand and 3056 (vs) cm^{-1} for the Ag(I) complex in the IR spectrum. For the benzimidazole molecule, these vibrational modes were observed at 3124, 3104, 3068, 3044, and 3016 cm^{-1} and were calculated at 3099, 3070, 3060, 3049, and 3039 cm^{-1}.[59]

3.2.3 | C-H in-plane and out-of plane bending vibrations

The in-plane bending vibrations are observed in the range of 1300–1000 cm^{-1}.[61] These vibrations were experimentally observed at 1194 (w), 1132 (w), and 1056 (s) cm^{-1} for the $[Ag(5ClBZ)_2(NO_3)]$ complex and at 1194 (w) and 1057 (s) cm^{-1} for the 5ClBZ molecule. The out-of plane bending vibrations are observed in the range of 1000–700 cm^{-1}.[62] For the 5ClBZ molecule and its silver nitrate complex, these vibration values were found at 847 (vs) and 845 (s) cm^{-1}, respectively. Also calculated at 861 and 792 cm^{-1} in the silver nitrate complex.

While the frequency values observed at 1273, 1202, 1157, 1135, and 1114 cm^{-1} were assigned as in-plane bending vibrations for the benzimidazole molecule, the frequency values observed at 933, 885, 769, and 749 cm^{-1} were assigned as out-of-plane bending vibrations.[59]

3.2.4 | C-C and C-N vibrations

In the IR spectrum, C-C and C-N stretching vibrations are observed in the regions of 1650–1200 cm^{-1}[63] and 1342–1266 cm^{-1},[64] respectively. Frequency values for the 5ClBZ molecule and the $[Ag(5ClBZ)_2(NO_3)]$ complex at which only C-C stretching vibrations were seen at 1631(w)/1626 (m), 1582(w)/1589(s), and 1272(m)/1273(m) cm^{-1}. Frequency values in which C-C and C-N vibrations are seen together (superimposed) are 1406 (s) and 1288 (s) cm^{-1} for the Ag(I) complex, 1478 (m), 1419 (m), and 1290 cm^{-1} for the free ligand. Other C-N stretching vibrations were observed for the free ligand at 1235 (m) and 1122 (w) cm^{-1}, while for its silver nitrate complex, 1226 (m) and 1114 (m) cm^{-1} were observed and calculated at 1239 and 1111/1114 cm^{-1}.

Finally, the C=N stretching vibration for the synthesized $[Ag(5ClBZ)_2(NO_3)]$ complex was observed at 1489 (s) cm^{-1} and calculated at 1492/1496 cm^{-1}. This vibration was observed at 1504 cm^{-1} in the IR spectrum of the free ligand. This shift in the C=N stretching vibration value indicates that the N atom in the imidazole ring of the 5ClBZ ligand is coordinated with the Ag atom.

In a previous study, the frequency values of the free indazole molecule and the synthesized silver nitrate complex were given. In this study, it was stated that the C=N stretching vibration observed at 1620 cm^{-1} for the indazole molecule shifted to 1630 cm^{-1} in its silver nitrate complex, and the reason for this shift was the coordination of the N atom and the Ag atom.[65] In another study in the literature, metal complexes of benzimidazole derivatives have been synthesized. It has been reported that the C=N stretching vibrations of the imine group of the free benzimidazole ligands were observed at 1631, 1639, 1633, and 1613 cm^{-1}, and these vibrational values of the synthesized metal complexes shift in the range of 6–35 cm^{-1}. Therefore, it was concluded that the N atoms in the imine group of the ligand are coordinated with the metals.[66]

3.2.5 | N-O vibrations

In the IR spectrum of the $[Ag(5ClBZ)_2(NO_3)]$ complex, two frequency values were observed at 1328 (s) and 1047 (m) cm^{-1}, which are not found in the spectrum of the free ligand. These frequency values belong to the N-O stretching vibration of the nitrate group. Another N-O

TABLE 1 Recorded and calculated IR frequencies of the $[Ag(5ClBZ)_2(NO_3)]$ complex and their assignments according to potential energy distribution (%), and measured IR frequencies of the 5CLBZ molecule.

Calculated				Observed		
Mode	**Fre**	**Fre[a]**	**I_{IR}[b]**	**IR 5CLBZ**	**IR $[Ag(5ClBZ)_2(NO_3)]$**	**TED[c]**
1	10	10	0.02			$38\delta_{NOH}$
2	19	19	0.20			$46\delta_{NOH} + 13\Gamma_{NCHO}$
3	20	20	0.09			$18\delta_{CHO} + 20\delta_{HON} + 19\Gamma_{CHON}$
4	25	24	1.04			$11\Gamma_{AgCCN} + 25\Gamma_{OHCN} +$
5	44	43	0.30			$22\delta_{CHO} + 20\Gamma_{CHON} + 20\Gamma_{HONO}$
6	55	55	0.13	50 w		$11\delta_{CHO} + 13\delta_{NOH} + 11\Gamma_{CHON}$
7	57	57	0.00		57 w	$11\upsilon_{OH} + 11\delta_{AgNC} + 18\delta_{OHC} + 13\Gamma_{OHCN}$
8	65	64	0.66			$21\upsilon_{AgO} + 46\delta_{OHC} + 11\Gamma_{CHON}$
9	72	71	2.09	76 vs	72 s	$10\delta_{AgNC} + 18\delta_{NOH} + 20\Gamma_{OHCN}$
10	89	87	0.17		86 m	$13\upsilon_{AgO} + 22\upsilon_{OH} + 38\delta_{AgNC}$
11	94	92	1.06	96 w	96 m	$17\delta_{NOH} + 11\Gamma_{OHCN} + 11\Gamma_{NCHO} + 28\Gamma_{AgCCN}$
12	118	116	1.76		109 m	$26\upsilon_{AgO} + 16\upsilon_{AgN} + 22\delta_{OHC} + 52\Gamma_{HONO}$
13	122	120	2.09			$62\upsilon_{OH}$
14	130	127	2.08	126 w	123 m	$52\Gamma_{CCCN} + 12\Gamma_{CNCC}$
15	133	130	2.48		137 m	$15\Gamma_{CCCN} + 16\Gamma_{CNCN} + 10\Gamma_{CNCC}$
16	165	162	3.42		150 m	$26\upsilon_{AgO} + 10\upsilon_{AgN} + 51\upsilon_{OH}$
17	202	199	0.60		203 w	$72\upsilon_{AgN}$
18/19	249/252	245/248	0.12			$10\Gamma_{CCCN} + 10\Gamma_{CNCN} + 22\Gamma_{CNCC}$
20	257	253	0.10	252 w	255 w	$67\delta_{ClCC}$
21	261	257	0.43			$61\delta_{ClCC}$
22/23	333	327	0.82			$67\Gamma_{CNCC}$
24/25	372	365	1.57	372 w	372 w	$45\upsilon_{ClC} + 24\delta_{CCC}$
26/22	429	422	1.26	422 w	416 w	$80\Gamma_{ClCCC}$
28/29	468	460	3.19		459 w	$61\delta_{CCN}$
30/31	499	491	1.66			$71\Gamma_{HNCN}$
32/33	598	588	4.76		591 m	$23\upsilon_{CN} + 10\upsilon_{ClC}$
34/35	606	596	5.58	596 s	608 s	$48\Gamma_{CCCN} + 12\Gamma_{CNCN}$
36/37	654	643	2.00	634 s		$22\Gamma_{HNCN} + 34\Gamma_{CNCN}$
38	713	701	0.35			$15\upsilon_{AgO} + 14\upsilon_{CC} + 62\delta_{ONO}$
39/40	714	702	2.52	711 s	710 m	$11\upsilon_{CC} + 12\upsilon_{ClC} + 12\delta_{NCN} + 22\delta_{ONO} + 14\delta_{CCC}$
41	722	710	5.55			$86\delta_{ONO}$
42/43	758	745	6.51	749 m	761 m	$20\Gamma_{CNCN} + 47\Gamma_{CNCC}$
44/45	806	792	8.03			$82\Gamma_{CCCH}$
46/57	809/810	796/797	6.74	797 vs	796 s	$24\upsilon_{CC} + 26\delta_{CNC}$
48	829	815	1.11		818 w	$98\Gamma_{OOON}$
49/50	876	861	5.12	847 vs	845 m	$82\Gamma_{CCCH}$
51/52	922	907	12.12	907 s	912s	$50\delta_{CCC}$
53/54	943	927	0.42			$67\Gamma_{NCHO} + 10\Gamma_{CNCN}$
55/56	948	932	1.96	932 m		$56\Gamma_{HCNC} + 12\Gamma_{CNCN}$
57/58	972/974	957	7.99	956 s	970 s	$67\delta_{CCC}$
59	1066	1047	5.40		1047 m	$81\upsilon_{NO}$

(Continues)

TABLE 1 (Continued)

Calculated				Observed		
Mode	**Fre**	**Fre[a]**	**I_{IR}[b]**	**IR 5CLBZ**	**IR [Ag(5ClBZ)$_2$(NO$_3$)]**	**TED[c]**
60/61	1073	1054	6.51	1057 s	1056 s	$11\delta_{CNC} + 13\delta_{CCC} + 20\delta_{CCH}$
62/63	1130	1111/1114	15.47	1122 w	1114 m	$42\upsilon_{CN} + 26\delta_{HNC} + 16\delta_{NCH}$
64/65	1150	1131	0.20		1132 w	$19\delta_{CCC} + 46\delta_{CCH}$
66/67	1206	1186	3.73	1194 m	1194 w	$19\delta_{CCH} + 12\delta_{NCH} + 12\delta_{CCN}$
68/69	1261	1239	4.12	1235 m	1226 m	$17\upsilon_{CN} + 49\delta_{CCH}$
70/71	1273/1276	1252/1254	18.28	1256 m	1253 m	$25\upsilon_{CN} + 11\delta_{CCC} + 23\delta_{HNC} + 11\delta_{NCH}$
72	1300	1278	23.76	1272 m	1273 m	$64\upsilon_{CC}$
73	1315	1293	7.07	1290 s	1288 s	$30\upsilon_{CC} + 21\upsilon_{CN} + 11\delta_{CCC} + 10\delta_{HCN}$
74	1319	1296	8.56		1328 s	$31\upsilon_{NO}$
75/76	1376	1353	6.88	1345 m	1344 s	$23\upsilon_{CC}$
77/78	1423	1399	9.35	1419 m	1406 s	$21\upsilon_{CC} + 15\upsilon_{CN} + 22\delta_{HNC}$
79/80	1480	1455	22.59			$12\upsilon_{CN} + 10\delta_{CNC} + 34\delta_{CCH}$
81	1490	1464	100.00	1464 m	1462 s	$12\upsilon_{CC} + 58\upsilon_{NO}$
82/83	1494	1469	1.62	1478 m		$11\upsilon_{CN} + 31\upsilon_{CC}$
84/85	1518/1522	1492/1496	9.77	1504 w	1489 s	$43\upsilon_{CN} + 21\delta_{HCN}$
86/87	1620	1593	8.27	1582 w	1589 s	$25\upsilon_{CC} + 22\delta_{CCC} + 13\delta_{CNC}$
88/89	1660	1631	5.97	1631 w	1626 m	$55\upsilon_{CC}$
90/91	3186	3062	9.96	3038 w	3056 vs	$88\upsilon_{CH}$
92/93	3208	3083	0.13			$94\upsilon_{CH}$
94/95	3209	3083	0.22			$90\upsilon_{CH}$
96/97	3219/3221	3094/3095	17.25	3088 vw	3146 vs	$97\upsilon_{CH}$
98/99	3655	3512	16.98			$99\upsilon_{NH}$

Note: υ: stretching, δ: in-plane bending, Γ: torsion, s: strong, m: medium, w: weak, v: very.

[a]Scaled wavenumbers calculated at B3LYP/6-311++G(d,p) using scaling factors 0.983for the wavenumber less than 1800 cm^{-1},[56]and 0.961 above 1800 cm^{-1}.[57]

[b]Relative absorption intensities normalized with highest peak absorption equal to 100.

[c]Total energy distribution level (TED) less than 10% are not shown.

stretching vibration for the title complex was also observed at 1462 (s) cm^{-1}. The calculated values corresponding to the experimental values are 1464, 1296, and 1047 cm^{-1}. In a study in the literature, the [Ag (methyl 4-pyridyl ketone)$_2$NO$_3$] complex was synthesized, and N-O stretching vibrations were reported for this structure at 1499, 1063, and 689 cm^{-1}.[57] The N-O stretching vibrations of the nitrate group of the $[C_{10}H_9N_3]_4AgNO_3$ complex synthesized in another study were observed at 1337 and 1196 cm^{-1} in the experimental IR spectrum.[67]

3.2.6 | C-Cl vibrations

The C-Cl stretching vibrations are observed generally as strong bands in the region 760–505 cm^{-1}. For the title complex, the peaks of C-Cl vibration were observed at 711, 591, and 372 cm^{-1} in the experimental IR spectrum, while this vibration was observed at 711 and 372 cm^{-1} in the free ligand. This vibration value of the 2-chloro benzimidazole molecule has been reported at 624 cm^{-1}.[16,68]

3.2.7 | Ag-N and Ag-O vibrations

For the [Ag(5ClBZ)$_2$(NO$_3$)] complex, some of the Ag-N and Ag-O vibrations were observed together at 150 (m) and 109 (m) cm^{-1}. The other Ag-N stretching vibration was measured at 203 (w) cm^{-1}, while the other Ag-O stretching vibration was measured at 86 cm^{-1}. Although not observed in the experimental spectrum, Ag-O stretching vibrations were also obtained at 701 and 64 cm^{-1} in theoretical calculations. Ag-N stretching vibrations for the [Ag (methyl 4-pyridyl ketone)$_2$NO$_3$] complex were observed as a weak band at 190 and 163 cm^{-1}.[57] In another study, one of the Ag-N vibrational bands of the synthesized $(C_{10}H_9N_3) \cdot AgNO_3$ complex was observed at 119 cm^{-1}.[68] Ag-O vibrations were also

measured at 124 and 100 cm^{-1} for the $AgNO_3$ complex of 2-methyl-quinoxaline.[69]

To determine the agreement between the experimental frequency values of the $[Ag(5ClBZ)_2(NO_3)]$ complex and the calculated frequency values, a correlation graph was drawn (Figure S3), and the R^2 value was determined for the grade line. The R^2 value is 0.9998, and this result shows that the experimental and calculated frequency values are highly compatible.

3.3 | ^{1}H NMR spectroscopy

NMR spectroscopy is one of the important tools used to determine the structure of organic and inorganic molecules. Therefore, the ^{1}H NMR spectra of the 5ClBZ molecule and the $[Ag(5ClBZ)_2(NO_3)]$ complex were recorded in DMSO solvent. Experimental and theoretical chemical shift values are listed in Table 2. In addition, ^{1}H NMR spectra are presented in Figure S4.

The experimental chemical shift values for the H atoms of the 5ClBZ molecule are (H_{10}) 7.60, (H_{12}) 7.66, (H_{13}) 8.14, and (H_{15}) 7.30 ppm. The theoretical values corresponding to these values are 7.78, 8.07, 8.28, and 7.56 ppm, respectively. In the experimental ^{1}H NMR spectrum of the synthesized $[Ag(5ClBZ)_2(NO_3)]$ complex, the chemical shift values (H_{10}/H_{25}) are 7.90/7.77, (H_{12}/H_{37}) 8.45, (H_{13}/H_{28}) 8.79/8.69, and (H_{15}/H_{30}) 7.39 ppm. The calculated values for these H atoms are 7.88, 8.20, 9.36, and 7.66 ppm, respectively.

When the ^{1}H NMR spectra of the free ligand and the synthesized title complex are compared, it is seen that the chemical shift values of the H_{12} and H_{13} atoms switch to a significantly higher value. In addition, similar results were obtained from theoretical calculations. These results show that the geometry of the synthesized complex was designed correctly.[70]

3.4 | Frontier molecular orbitals (FMOs) and UV-Vis analyses

The frontier molecular orbitals, called the highest occupied molecular orbital (HOMO) and the lowest occupied molecular orbital (LUMO), are the most important features used to determine the electrical and optical properties of a molecule. It is also known as the electron-donating ability of the HOMO molecule and the electron-receiving ability of the LUMO molecule.[71,72] After determining the energy values of these two molecular orbitals, the energy values of the other quantum chemical properties such as ionization potential (I), electron affinity (A), global hardness (η), electronegativity (χ), chemical potential (μc), global softness (σ), and global electrophilicity (ω) can be calculated with the following equations[73]:

$$I = -E_{HOMO} \tag{4}$$

$$A = -E_{LUMO} \tag{5}$$

$$\eta = \frac{(-E_{HOMO} + E_{LUMO})}{2} \tag{6}$$

$$\chi = -\mu_c \tag{7}$$

$$\mu_c = \frac{(E_{HOMO} + E_{LUMO})}{2}\mu \tag{8}$$

$$\sigma = 1/\eta \tag{9}$$

$$\omega = \frac{(\mu_c{}^2)}{2\eta} \tag{10}$$

All the above quantum chemical properties are given in Table 3. HOMO has a value of −6.57 eV, and LUMO has a value of −1.21 eV for the 5ClBZ molecule. The energies of these two molecular orbitals are −5.92 and −1.69 eV for the $[Ag(5ClBZ)_2(NO_3)]$ complex. The energy gaps calculated for the free ligand and its Ag(I) complex to donate electrons from the HOMO orbital with a higher number of electrons with more energy to the LUMO orbital with fewer electrons with lower energy are 5.36 and 4.23 eV, respectively. Also, the global hardness energy values of the 5ClBZ molecule and the $[Ag(5ClBZ)_2(NO_3)]$ complex are 2.68 and 2.11 eV, respectively. These band gaps and global hardness values confirm that both the

TABLE 2 Experimental and theoretical chemical shift values of the 5ClBZ molecule and the $[Ag(5ClBZ)_2(NO_3)]$ complex.

Ligand			Complex		
Atoms	**Experimental**	**Calculated**	**Atoms**	**Experimental**	**Calculated**
H_{10}	7.60	7.78	H_{10}/H_{25}	7.90/7.77	7.88
H_{12}	7.66	8.07	H_{12}/H_{37}	8.45	8.20
H_{13}	8.14	8.28	H_{13}/H_{28}	8.79/8.69	9.36
H_{15}	7.30	7.56	H_{15}/H_{30}	7.39	7.66

TABLE 3 The quantum chemical properties and energy values from the DFT calculations of the 5ClBZ molecule and the $[Ag(5ClBZ)_2(NO_3)]$ complex.

Molecular Orbitals	Energy (eV)			Energy gap (eV)		Ionization potential (I) (eV)		Electron affinity (A) (eV)		Global hardness (η) (eV)		Electronegativity (χ) (eV)		Chemical potential (μ_c) (eV)		Global softness (σ) $(eV)^{-1}$		Global electrophilicity (ω) (eV)	
	a	b		a	b	a	b	a	b	a	b	a	b	a	b	a	b	a	b
H	−6.57	−5.92	ΔE_{H-L}	5.36	4.23	6.57	5.92	1.21	1.69	2.68	2.11	3.89	3.81	−3.89	−3.81	0.37	0.47	2.82	3.43
L	−1.21	−1.69																	
H − 1	−6.80	−7.00	$\Delta E_{H-1-L+1}$	6.14	5.31	6.80	7.00	0.66	1.69	3.07	2.65	3.73	4.34	−3.73	−4.34	0.33	0.38	2.26	3.56
L + 1	−0.66	−1.69																	
H − 2	−7.99	−7.07	$\Delta E_{H-2-L+2}$	7.74	6.23	7.99	7.07	0.25	0.84	3.87	3.11	4.12	3.95	−4.12	−3.95	0.26	0.32	2.19	2.51
L + 2	−0.25	−0.84																	

Note: H: HOMO (highest occupied molecular orbital), L: LUMO (lowest unoccupied molecular orbital), eV: electron volt, $(eV)^{-1}$: 1/eV.

[a]Energy values for 5ClBZ molecule.

[b]Energy values for $[Ag(5ClBZ)_2(NO_3)]$ complex.

5ClBZ molecule and the $[Ag(5ClBZ)_2(NO_3)]$ complex are very stable, and charge transfers occur within molecules. When the energy gap values and global hardness values of the free ligand and the synthesized complex are compared, the $[Ag(5ClBZ)_2(NO_3)]$ complex has a softer structure than the free ligand.[74,75]

HOMO and LUMO graphs are presented in Figure 4. For the 5ClBZ molecule, HOMO was distributed over the entire molecule, while for the $[Ag(5ClBZ)_2(NO_3)]$ complex, it was distributed over the Ag atom and NO3 group in the structure. The LUMO orbitals for both the free ligand and the Ag(I) complex were also distributed over the entire ligand, except for the Cl atom.

Also, the UV-Vis spectrum of the free ligand and its Ag(I) complex was recorded and presented in Figure 5. While absorbance peaks were observed at 214, 244, 280, and 286 nm for the 5ClBZ molecule, the absorbance peaks for the $[Ag(5ClBZ)_2(NO_3)]$ complex were observed at 223, 254, 278, and 286 nm. When the absorbance peaks of the 5ClBZ molecule and $[Ag(5ClBZ)_2(NO_3)]$ complex were compared in the experimental UV-Vis spectrum, it was determined that the peaks obtained at 214 and 244 nm for the free ligand shifted to 223 and 254 nm, respectively. This shift in the absorbance peaks is an indication that the free ligand and the Ag atom are coordinated.[65] The experimental bands of the ligand and silver complex are mainly due to $H-1 \rightarrow L$ and $H-3 \rightarrow L-3$ excitations (Table 4), which are assigned to $\pi \rightarrow \pi^*$ and $n \rightarrow \pi^*$ transitions, respectively.

3.5 | MEP analysis

The molecular electrostatic potential map is a tool used to determine the reactive regions of a molecule using theoretical computational methods.[76] Colored MEP surfaces created according to electrostatic potential increasing in the order of blue < green < yellow < orange < red are presented in Figure 6.[77] When the MEP map of the 5ClBZ molecule is examined, it is seen that the red-colored region (mostly negative) is distributed around the N_2 atom. In addition, the Cl atom is in the yellow region, which is less electron-rich than the red color. According to the MEP map of the $[Ag(5ClBZ)_2(NO_3)]$ complex, it is observed that the most negative region is distributed over the O atoms of the NO_3 group. In addition, as a result of the coordination of the N atoms with a negative value with the Ag atom with a positive value, they are now in the positive, that is, blue-colored region. In a study in the literature, the silver nitrate complex of thiourea was synthesized, and a MEP map was created. In this map, the most negative region (electrophilic) showed a distribution on the nitrate group, while the most positive region

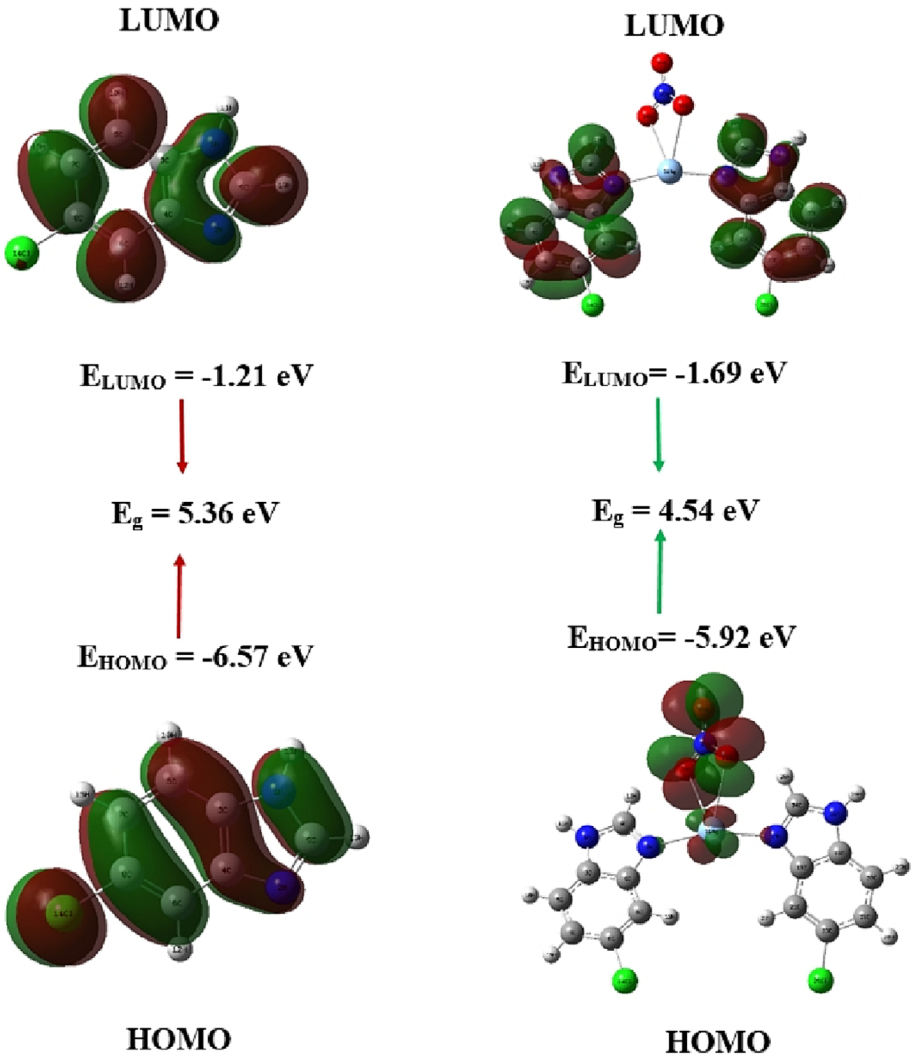

FIGURE 4 The HOMO-LUMO diagram of the 5ClBZ molecule and the $[Ag(5ClBZ)_2(NO_3)]$ complex.

(nucleophilic) showed a distribution on the Ag atom.[78] Similar results are available in other studies in the literature.[57]

3.6 | Charge and Fuki function analysis

Determining the atomic charge and Fukui function values of a molecule are very important because they are related to electronics, dipole moment, molecular polarizability properties, and other molecular properties.[79,80] In this study, APT, NBO, and Hirshfeld charge and Fukui function analyses of the 5ClBZ molecule and its $[Ag(5ClBZ)_2(NO_3)]$ complex were theoretically performed. The charge values of the 5ClBZ molecule and the $[Ag(5ClBZ)_2(NO_3)]$ complex are listed in Table S2 and presented in Figure 7.

According to the three different charge analyses of the 5ClBZ molecule, the atoms with the most negative charge are the N_1 and N_2 atoms. In addition, the Cl_{14} atom and the C_6 and C_7 atoms also have negative values. When the charge analysis of the $[Ag(5ClBZ)_2(NO_3)]$ complex was examined, N_1, N_2, N_{16}, and N_{17} and O_{32}, O_{33}, and O_{34} atoms belonging to the nitrate group were determined to have the most negative values. In addition, C_6, C_7, C_{21}, and C_{27} atoms in the complex structure were also found to be negative. The Ag_{31} atom and N_{35} atom in the complex were found to be the atoms with the most positive value according to all three charge methods. These results obtained from load analyses are also very compatible with each other when compared with MEP maps.

Fukui functions were calculated with the following equations to determine the neutral, nucleophilic, and electrophilic attack values of the 5ClBZ molecule and the $[Ag(5ClBZ)_2(NO_3)]$ complex from the Hirshfeld charges of the neutral, cation, and anion states.[81,82]

$$f_k{}^0 = (1/2)[q_k(N+1) - q_k(N-1)] \quad \text{neutral attack} \quad (11)$$

$$f_k{}^+ = q_k(N+1) - q_k(N) \quad \text{nucleophilic attack} \quad (12)$$

$$f_k{}^- = q_k(N) - q_k(N-1) \quad \text{electrophilic attack} \quad (13)$$

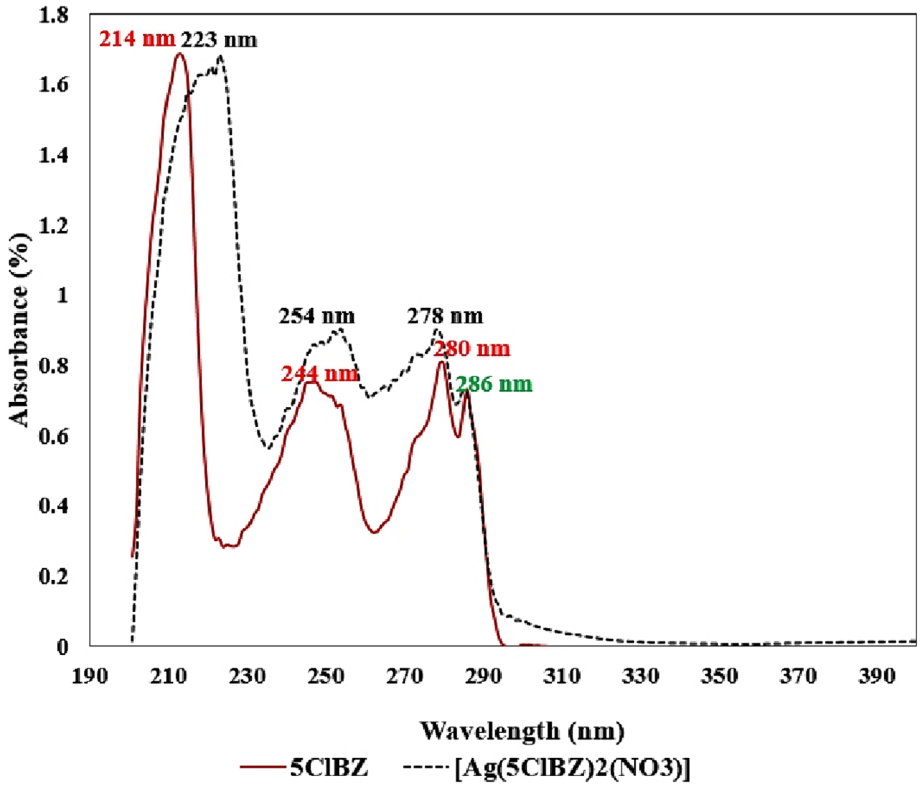

FIGURE 5 Experimental UV-Vis spectra of the 5ClBZ molecule and the $[Ag(5ClBZ)_2(NO_3)]$ complex.

TABLE 4 UV-Vis absorption wavelengths, excitation energy, oscillator strength and major contribution values of 5ClBZ molecule and the $[Ag(5ClBZ)_2(NO_3)]$ complex.

Compound	Exp. λ_{max} (nm)	Theo. λ_{max} (nm)	*E* (eV)	*f*	Symmetry	Major contributions
5ClBZ	280	261	4.75	0.0885	Singlet-A	HOMO−1/LUMO+1
	244	242	5.12	0.0793	Singlet-A	HOMO−1/LUMO HOMO/LUMO
	214	204	6.07	0.6107	Singlet-A	HOMO/LUMO HOMO−1/LUMO
$[Ag(5ClBZ)_2(NO_3)]$	280	263	4.71	0.2210	Singlet-A	HOMO−1/LUMO+1
	254	246	5.02	0.1093	Singlet-A	HOMO−4/LUMO+1
	223	226	5.48	0.0781	Singlet-A	HOMO−3/LUMO+3

The q_kN, $q_k(N+1)$, and $q_k(N-1)$ in these equations are the total charge amounts in the *r*th atom in the neutral, cationic, and anionic states, respectively. Also, a new descriptor $\Delta f(r)$, called the dual descriptor, was proposed to predict nucleophilic and electrophilic regions by[83]

$$\Delta f(r) = f^+(r) - f^-(r) \quad (14)$$

According to this equation, if $\Delta f(r) > 0$, the region is favored for nucleophilic attack, and if $\Delta(f) < 0$ the region is preferred for electrophilic attack. In other words, when $\Delta f(r) > 0$, the region is electrophilic, and when $\Delta(f) < 0$, the region is nucleophilic.[84] Fukui function values for the 5ClBZ molecule and the $[Ag(5ClBZ)_2(NO_3)]$ complex are presented in Table S3, and dual descriptor maps designed using the Multiwfn program are presented in Figure 8.[43]

In Figure 8, the blue and yellow colors represent electrophilic and nucleophilic regions, respectively. In the image created for the 5ClBz molecule, it was determined that N_1, C_3, C_8, and Cl_{14} atoms are electrophilic. In the image created for the $[Ag(5ClBZ)_2(NO_3)]$ complex, it was determined that the oxygen atoms of the nitrate group (O_{32}, O_{33}, and O_{34}) and the C_3, C_8, C_{18}, C_{23}, Cl_{14}, and Cl_{29} atoms were electrophilic. These images created with Multivfn are also in harmony with the results obtained from the Fukui functions calculated with the Gaussian 09W

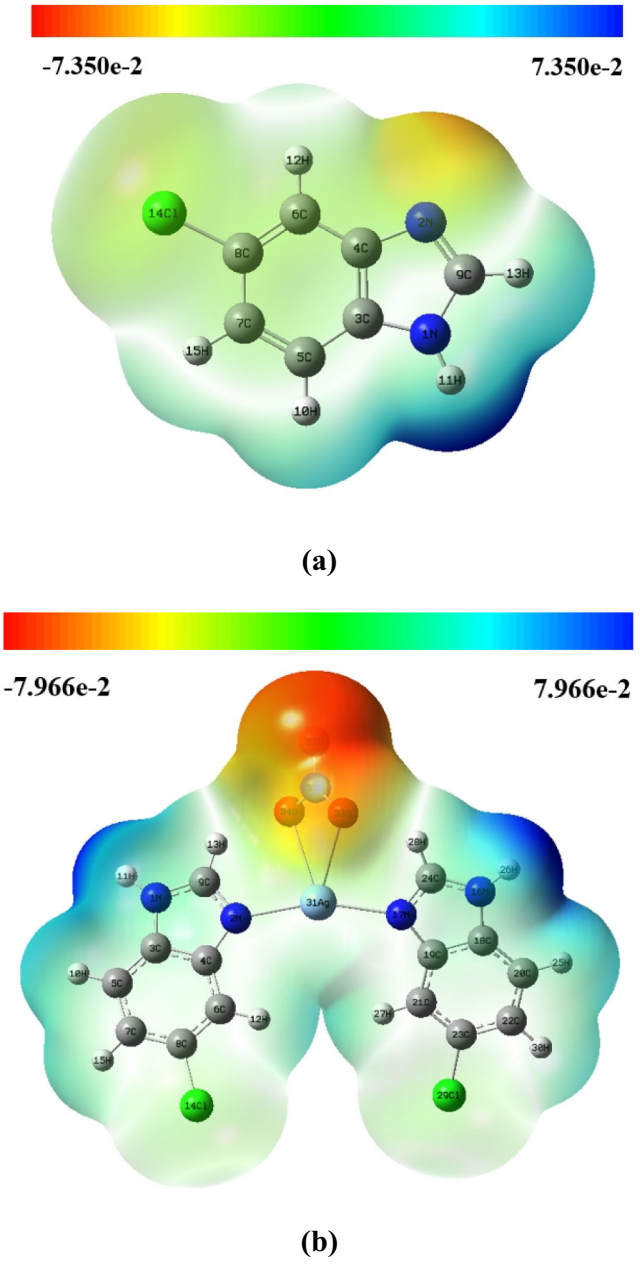

FIGURE 6 Molecular electrostatic potential surface (MEP) maps of the 5ClBZ molecule (a) and the $[Ag(5ClBZ)_2(NO_3)]$ complex (b).

package program. In addition, the results obtained for the Fukui functions are also in good agreement when compared with the MEP map and charge analyses.

3.7 | In vitro biological activity

3.7.1 | Antidiabetic activity (α-amylase enzyme inhibition)

The enzymes that enable the breakdown of starch into glucose are α-amylase and α-glycosidase.[85,86] Therefore, inhibitors of these enzymes have important functions in the control of diabetes.[87] Therefore, inhibition of these enzymes is important. α-amylase enzyme inhibition percentages and IC_{50} values of 5CIBZ, $[Ag(5ClBZ)_2(NO_3)]$, and standard acarbose are shown in Table 5 and Figure 9.

In this study, α-amylase enzyme inhibition IC_{50} values were determined as 5CIBZ (189.87 μg/mL), $[Ag(5ClBZ)_2(NO_3)]$ (126.75 μg/mL), and standard acarbose (28.96 μg/mL). It was determined that the antidiabetic capacity of the Ag-benzimidazole complex was stronger than that of the 5CIBZ ligand. The results were compared with standard acarbose.

The antioxidant and antidiabetic capacities of benzimidazole-based Cu and Zn complexes were investigated. As a result of this study, the in vitro antidiabetic activity of benzimidazole complexes was expressed with IC_{50} values. Complex 1 (0.74 mg/mL) and complex 2 (1.00 mg/mL) were designated as standard acarbose (2.34 mg/mL). α-amylase activity from the Zn complex was not determined. It has been reported that copper complexes exhibit more effective antidiabetic activity than standard acarbose and the ligand benzimidazole (39.87 mg/mL).[88] In a study, the in vitro α-amylase inhibition of 31 arylated and hetero-arylated benzimidazoles was examined. It has been reported that the enzyme inhibition IC_{50} values of the samples ranged between 1.86 ± 0.08 and 3.16 ± 0.31 μM.[89] The antidiabetic activities of 10 benzimidazole-substituted coumarin-3-carboxamide substances were measured. It was determined that α-amylase enzyme inhibition IC_{50} values ranged between 67.52 and 105.86 μM.[90] It was seen that our results were compatible with the studies performed.

3.7.2 | Antioxidant activity ($DPPH^{\bullet}$ and $ABTS^{\bullet+}$ radicals scavenging activity)

The antioxidant capacities of the samples were determined by looking at their radical scavenging activities. The percentages of inhibition of these radicals and IC_{50} values of the samples were determined. Standard BHT material was used to compare the results. The results are expressed in Table 6 with Figure 10.

The IC_{50} (50% inhibitory concentration) value is called the amount of antioxidant substance that reduces the initial DPPH radical concentration of the samples by 50%. A low IC_{50} value indicates high antioxidant activity.[91,92] The IC_{50} results of 5CIBZ, $[Ag(5ClBZ)_2(NO_3)]$, and standard BHT samples were found to be 150.67, 105.62, and 18.39 μg/mL, respectively. In a study examining the DPPH radical scavenging effect of benzimidazole-based Cu and Zn complexes, the IC_{50} values were determined to be

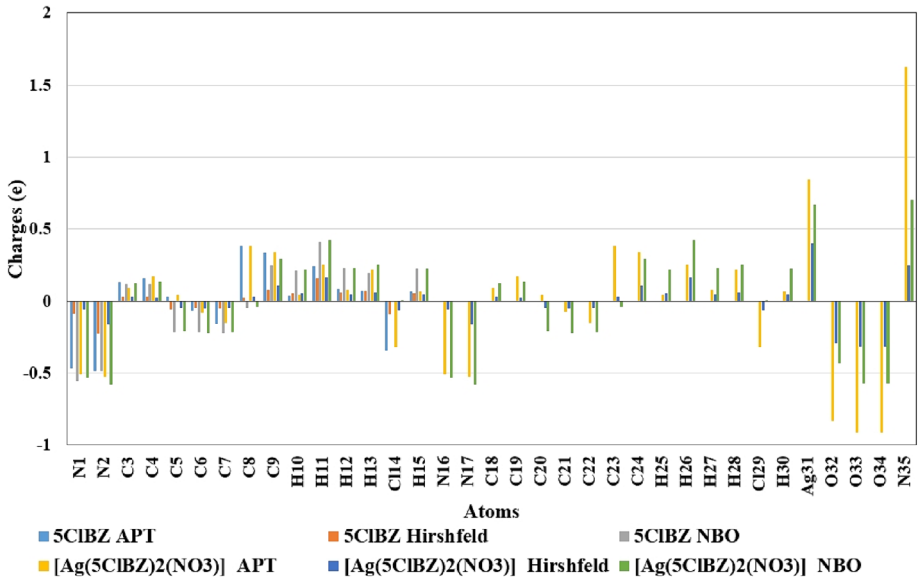

FIGURE 7 Charge graphics of the 5ClBZ molecule and the [Ag $(5ClBZ)_2(NO_3)$] complex.

copper complex 1 (43.72 μg/mL), copper complex 2 (43.76 μg/mL), and standard vitamin C (5.63 μg/mL).[88] In one study, the in vitro scavenging capacities of 31 arylated and hetero-arylated benzimidazoles against these two radical types were examined. Moreover, IC_{50} values of $DPPH^{\bullet}$ and $ABTS^{\bullet+}$ radical scavenging capacities have been reported to range from (1.36 ± 0.09–3.60 ± 0.20 μM) and (1.37 ± 0.21 to 4.00 ± 0.10 μM), respectively.[89] In a study, the antioxidant activities of benzimidazole-substituted coumarin-3-carboxamide substances were examined. As a result, the scavenging activities of 10 substances on these two different radicals were determined. It has been reported that $DPPH^{\bullet}$ radical scavenging IC_{50} results vary between (89.67 and 145.21 μM) and $ABTS^{\bullet+}$ radical scavenging values (93.45 and 143.5 μM).[90] Our study results were found to be compatible with the literature.

3.8 | In silico biological activity

3.8.1 | Molecular docking studies

Molecule activities have been analyzed using Gaussian calculation results, but this method is insufficient. To completely analyze the activity of the compounds, molecular docking calculations were undertaken. To corroborate the experimental study on the biological activities of the free ligand and Ag(I) complex, we have chosen appropriate receptors and docked these molecules against them. In our study, the antioxidant and antidiabetic abilities of the title compounds were elucidated.

Molecular docking with the α-amylase enzyme

Pancreatic enzyme α-amylase typically breaks down polysaccharides into short-chain carbs, allowing them to pass across the blood–brain barrier more easily. In patients with type II diabetes, however, α-amylase must be inhibited or delayed in order to prevent hyperglycemia.[35] The molecular docking study of the compounds with alpha-amylase (PDB ID: 2VQ4) was conducted in an effort to determine the compounds' suitability with respect to the chosen protein target and antidiabetic potential.[93]

The docking properties, including the free energy of binding and inhibition constant (K_i), along with the extent of hydrogen bonding interactions, are summarized in Table 7. The results showed that both standard drug acarbose and title compounds were able to bind to the active site of α-amylase, the calculated binding energy was found to be −9.1 and −4.9, −10.1 kcal/mol, respectively, for acarbose and title compounds. A stable complex-enzyme complex forms when the binding affinity between the Ag(I) complex molecules and receptor protein is stronger, which is correlated with a lower binding free energy. That is consistent with the findings of in vitro investigations. The results revealed that title compounds have a high binding affinity when compared with the standard drug acarbose, which are consistent with the findings of in vitro research. The analytical expression of IC_{50} for different types of inhibition is related to the apparent computed inhibitory constants (calc. K_i).[94] Determining these values indicates that at a fixed substrate concentration the lower the IC_{50} and Ki, the stronger the inhibitor, and the less drug is needed to inhibit enzyme activity. The antidiabetic capacity of the

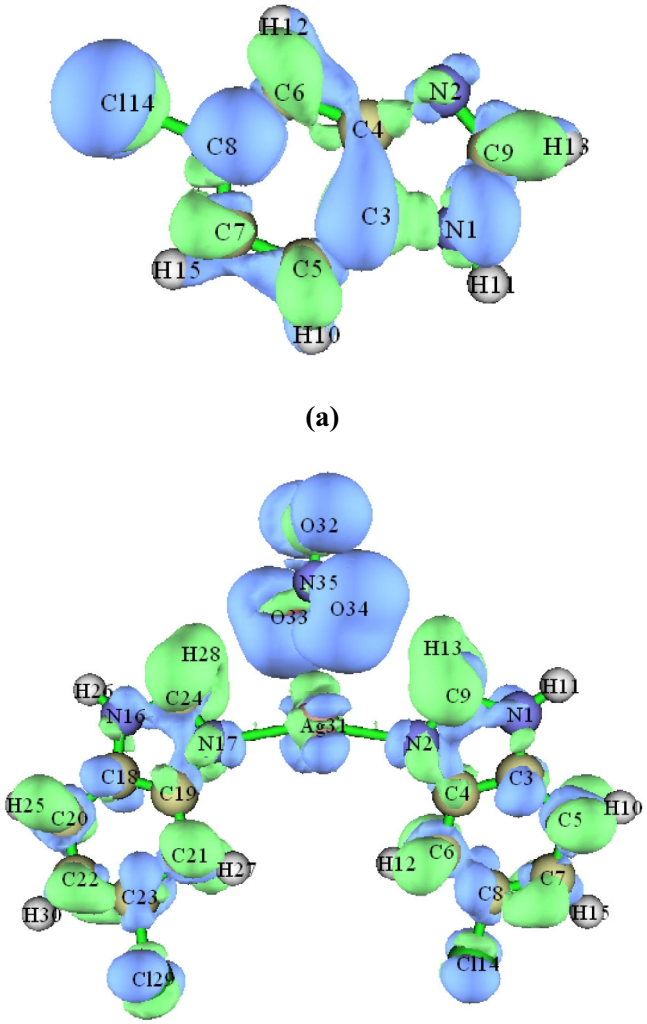

FIGURE 8 Dual descriptor graphics for Fukui functions of the 5ClBZ molecule (a) and the $[Ag(5ClBZ)_2(NO_3)]$ complex (b).

Ag(I) complex was found to be greater than that of the free ligand. The results were compared with those obtained with the reference drug acarbose. Docking results reveal that lowering the binding energy value lowers the inhibitor constant (K_i), which enhances biological activity, and Figure 11 shows the surface diagram indicating the docking interactions between the active site and each title compounds. The free ligand created strong hydrogen bond contact with GLU'233 and ILE'235 in the active site of the human pancreatic α-amylase enzyme. This strong interaction was a hydrogen donor between the N-atom of the imidazole ring and GLU'233 and ILE'235 residues. Also, the binding of the Ag(I) complex with amino acids (TYR'62, HIS'101, ARG'195, ASP'300) and the presence of the -OH group formed by the enzyme with this nitrate group increases the antidiabetic activity. While the other type of interaction was π–H between the benzene ring and HIS'235 over a distance of 3.54 Å, halogen bands were displayed between the Cl atom and GLU'233 (2.81 Å).

Molecular docking with antioxidant enzyme

Antioxidant agents mainly function as electron acceptors or hydrogen donors at the reactive site to eliminate free radicals. Thus, to develop novel therapeutic drugs to eliminate the damage or impact caused by free radicals is to achieve greater awareness.[95] So, in this regard, a molecular docking study was performed to analyze the binding modes of the studied compound against the antioxidant enzyme (PDB ID: 3NM8). The calculated docking parameters, contact area, and Ki values of both compounds compared with the standard compound (ascorbic acid) are shown in Table 7, while the binding interactions are shown in Figure 11. The results showed that both the ligand and its Ag(I) transition metal complex could bind

TABLE 5 α-amylase enzyme inhibition percentages with IC_{50} values of the samples.

Samples	Concentration (μg/mL)	α-amylase % inhibition	IC_{50} (μg/mL)
5CIBZ	25	18.25 ± 1.28	189.87
	50	24.41 ± 1.38	
	100	32.72 ± 1.05	
$[Ag(5ClBZ)_2(NO_3)]$	25	24.55 ± 1.59	126.75
	50	32.09 ± 1.35	
	100	43.17 ± 1.43	
Standard (Acarbose)	25	46.84 ± 1.56	28.96
	50	59.24 ± 1.24	
	100	70.13 ± 1.48	

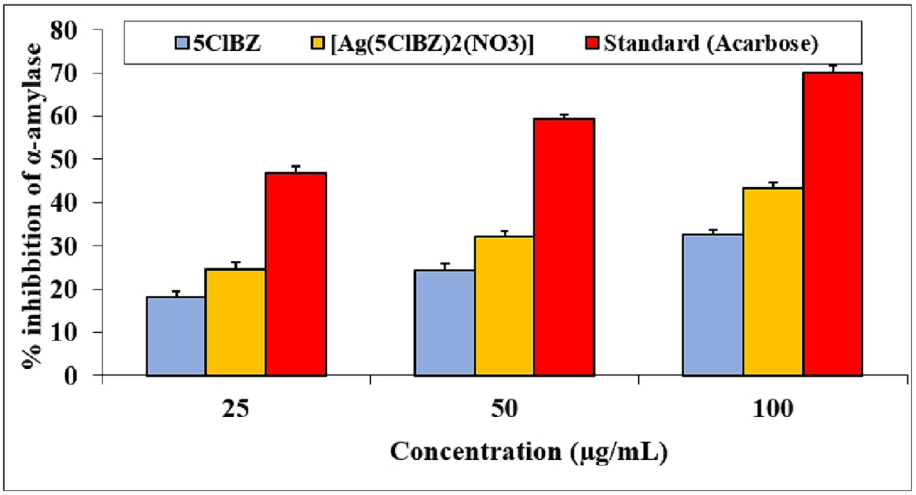

FIGURE 9 α-amylase enzyme inhibition percentages of the samples.

TABLE 6 Inhibition percentages with IC_{50} values of the samples against $DPPH^{\bullet}$ and $ABTS^{\bullet+}$ radicals.

Samples	Concentration (µg/mL)	% inhibition of $DPPH^{\bullet}$	IC_{50} (µg/mL)	% inhibition of $ABTS^{\bullet+}$	IC_{50} (µg/mL)
5CIBZ	25	18.89 ± 1.03		14.98 ± 1.68	
	50	29.43 ± 1.37	150.67	27.12 ± 1.38	165.78
	100	37.27 ± 1.62		33.55 ± 1.58	
[Ag $(5ClBZ)_2(NO_3)$]	25	23.38 ± 1.05		21.33 ± 1.49	
	50	38.11 ± 1.71	105.62	35.16 ± 1.47	113.48
	100	46.87 ± 1.44		44.73 ± 1.27	
Standard (BHT)	25	48.82 ± 1.64		47.42 ± 1.59	
	50	69.22 ± 1.31	18.39	65.91 ± 1.44	23.29
	100	82.33 ± 1.43		75.93 ± 1.48	

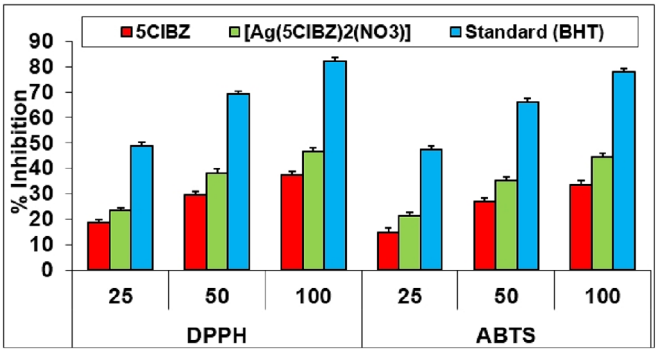

FIGURE 10 Percent inhibition values of samples against $DPPH^{\bullet}$ and $ABTS^{\bullet+}$ radicals.

to the active site of the enzyme. When the binding of the title compounds was compared with the standard antioxidant ascorbic acid, it was found that both compounds had strong antioxidant properties. Whereas, the silver complex was found to have the best docking score (−8.8 kcal/mol) but was less effective as an antioxidant (inhibition constant $K_i = 464.62$ µM). Interactions showing that proteins are inhibited due to the interaction of molecules with proteins are given in Figure 11. In general, these interactions are chemical interactions, and they are hydrogen bonds, polar and hydrophobic interactions, π-π, and halogen. The free ligand and its silver complex were found to hydrogen bond with the nitrogen atom in the imidazole ring, VAL'217 and ASP'36 residues (Figure 11). Additional hydrophobic contacts were discovered with ALA'40, ALA'44, LYS'47, GLY'43, ILE'139, VAL'218, ARG'209, and ALA'221.

3.8.2 | Physicochemical characteristics

Pharmacokinetic analysis should be performed to better understand the usefulness of a compound in terms of its potential application as a drug or supplement due to its fingerokinetic parameters and drug-like properties. The analysis is based on the calculation of some important physiochemical parameters described by the structure of a particular compound.[96,97] Therefore, to discover

TABLE 7 Docking parameters of the interaction compound with receptors.

Receptor	Compounds	H-bonded residues	Bonded distance (Å)	Binding Energy (kcal/mol)	Inhibition constant K_i (μM)
2QV4	5CIBZ	LYS 200, GLU 233,ILE 235	3.22, 2.30, 2.17	−4.9	237.06
	[Ag $(5ClBZ)_2(NO_3)$]	TYR 62, HIS 101, ARG 195, ASP 300	2.08, 2.87 2.38, 2.91	−10.1	45.14
3NM8	Acarbose[a]	GLN 63, TRP 59, ASN 105, ALA 106 VAL 107, THR 163 GLY 164, GLU 233 ASP 300, TYR 62		−9.1	
	5CIBZ	HIS 42, HIS 60, HIS 204, VAL 217	3.64, 2.52, 3.542.95	−5.5	197.90
	[Ag $(5ClBZ)_2(NO_3)$]	ASP 36, ASP 140	2.29, 2.25	−8.8	464.62
	Ascorbic acid[a]			−4.4	

[a]Standard drug: acarbose, ascorbic acid.

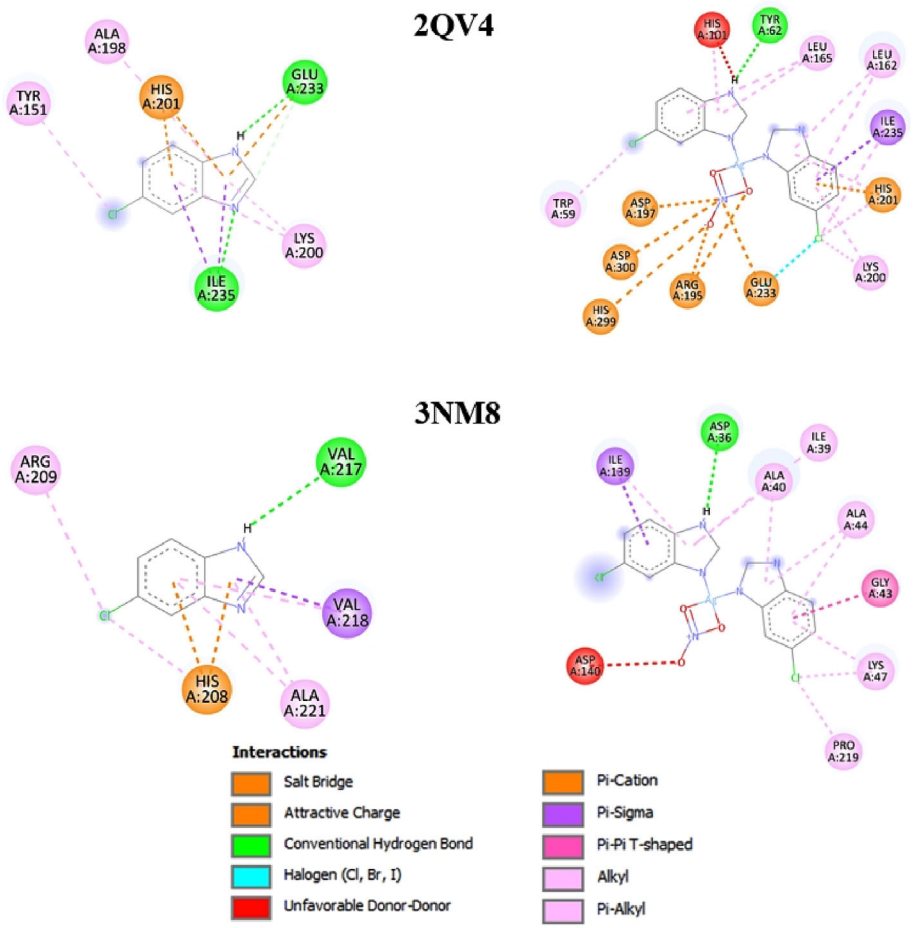

FIGURE 11 Two-dimensional view of intermolecular interactions with an enzyme and different amino acids (a) free ligand (5CIZB), (b) Ag(I)-Complex.

the drug-like properties of the molecules we studied, we examined whether they complied with Lipinski's rule of five for drug likeliness. The free ligand and its Ag(I) complex were compared with known standard reference drugs Acarbose and Ascorbic Acid, and their drug-likeness was evaluated according to Lipinski's rule. According to the predicted results, all compounds qualify as orally active drugs as they adhere to "Lipinski's rule of five" criteria (lipophilicity (LogP) ≤ 5, HBD ≤ 5, HBA ≤ 10, molecular weight (g/mol) ≤ 500 g/mol, polarity: 20 Å ≤ TPSA (Å2) ≤ 140 Å, and flexibility (rotatable bonds): <9), molar refractivity in the range of 40–130.[96,98]

TABLE 8 Physiochemical descriptors (Lipinski's rule of five) of compounds.

Compounds	Mol.Wt	H-bond acceptor	H-bond donor	No: of rotating bond	TPSA (A^2)	Log P	Molar refractivity
5CIBZ	152.58	1	1	0	28.68	2.22	41.10
$[Ag(5ClBZ)_2(NO_3)]$	478.06	6	5	2	113.69	0.68	110.25
Acarbose[a]	645.11	19	14	9	321.17	−6.94	136.69
Ascorbic acid[a]	176.126	6	3	2	107.22	−1.41	35.12

[a]Drugs reference, topological polar surface area (TPSA); number of rotatable bonds (n-rotb); molecular weight (Mol.Wt).

TABLE 9 Pharmacokinetic/ADMET parameters of compounds.

Compounds	GIA	BBB permeant[a]	HIA absorption[b]	Caco-2 permeability[c] (nm/s)	Log Kp (cm/s)[d]	Toxicity Class
5CIBZ	High	4.82	93.25	43.39	−5.05	II
$[Ag(5ClBZ)_2(NO_3)]$	High	0.51	98.52	68.66	−6.08	III

Abbreviations: BBB, blood–brain barrier; Caco-2 (colorectal carcinoma), cell permeability; GIA, gastrointestinal absorption; HIA, human intestinal absorption; Log Kp, skin permeation value.
[a]Predicted brain/blood partition coefficient (acceptable range: −3.0 to 1.2).
[b]Percentage of human Intestinal absorption (<25% is poor and >80% is high).
[c]Predicted Caco-2 cell permeability in nm/s (acceptable range: <25 is poor and > 500 is great).
[d]Predicted skin permeability (acceptable range: −8.0 to −10 cm/h).

Class I: fatal if swallowed (LD50 ≤ 5)
Class II: fatal if swallowed (5 < LD50 ≤ 50)
Class III: toxic if swallowed (50 < LD50 ≤ 300)
Class IV: harmful if swallowed (300 < LD50 ≤ 2000)
Class V: may be harmful if swallowed (2000 < LD50 ≤ 5000)
Class VI: non-toxic (LD50 > 5000)

TABLE 9 (Continued)

Compounds	LD_{50} (mg/kg)	Hepatotoxicity	Carcinogenicity	Immunotoxicity	Mutagenicity	Cytotoxicity
5CIBZ	8	Inactive (0.53)	Inactive (0.59)	Inactive (0.99)	Inactive (0.77)	Inactive (0.77)
$[Ag(5ClBZ)_2(NO_3)]$	75	Inactive (0.59)	Inactive (0.51)	Inactive (0.89)	Inactive (0.52)	Inactive (0.61)

Abbreviations: BBB, blood–brain barrier; Caco-2 (colorectal carcinoma), cell permeability; GIA, gastrointestinal absorption; HIA, human intestinal absorption; Log Kp, skin permeation value.
[a]Predicted brain/blood partition coefficient (acceptable range: −3.0 to 1.2).
[b]Percentage of human Intestinal absorption (<25% is poor and >80% is high).
[c]Predicted Caco-2 cell permeability in nm/s (acceptable range: <25 is poor and > 500 is great).
[d]Predicted skin permeability (acceptable range: −8.0 to −10 cm/h).

- Class I: fatal if swallowed (LD50 ≤ 5)
  - Class II: fatal if swallowed (5 < LD50 ≤ 50)
  - Class III: toxic if swallowed (50 < LD50 ≤ 300)
  - Class IV: harmful if swallowed (300 < LD50 ≤ 2000)
  - Class V: may be harmful if swallowed (2000 < LD50 ≤ 5000)
  - Class VI: non-toxic (LD50 > 5000)

As can be seen from Table 8, the studied compounds did not show any violations of the Lipinski rules, and these results showed that the drugs had good bioavailability. Furthermore, this behavior is similar to that of ascorbic acid, but it is superior to acarbose, which exhibited a violation of Lipinski's rule in Table 8.

3.8.3 | Pharmacokinetic analysis

The identification of a medicine is a significant step, but it is not adequate because the drug may be toxic or have poor ADMET properties. Predicting ADMET characteristics is crucial to avoiding complications during clinical

studies.[99] Therefore, we had some of the characteristic features of ADMET parameters calculated to evaluate the potential of the studied molecules to act as drug precursors. The parameters presented in Table 9 indicate that the blood–brain barrier (BBB) serves as the primary interface between the blood circulation and the central nervous system. This characteristic is critical as it dictates whether drugs can traverse the BBB and, consequently, whether they can exert their intended effect on the brain. It has been observed that the BBB permeability for the Ag(I) complex indicates the capability of the compound to pass through the blood/brain barrier. The observations revealed that both compounds can be absorbed in the human intestine (HIA) and are also permeable for Caco-2 cells. Title compounds showed high gastrointestinal absorption (GI) and the lowest ability to penetrate through the skin. On the other hand, the compounds examined in the toxicity profile were classified as toxicity classes 2 and 3. This indicates that they may be toxic if swallowed. As a result, they do not cause any mutagenic, cytotoxic, tumorigenic, or immunotoxic effects. These results indicate that the title compounds have good ADMET parameters and may be conductive candidates as drugs.

4 | CONCLUSION

A new metal complex containing 5-chlorobenzimidazole was produced and characterized utilizing chemical analyses and spectroscopic methods (FT-IR, ^{1}H-NMR, UV-Vis). HOMO-LUMO calculations show that the complex is more stable than the free ligand, has biological character, and experiences intermolecular interactions. The MEP visual depiction is used to locate the molecule's reactive areas. These areas are more electrophilic and closer to the Ag atom and nitrate group, allowing them to interact with amino acid-containing proteins. As a result of careful evaluation of molecular docking studies, in vitro screening test, and comparison results with standard antidiabetic acarbose and antioxidant ascorbic acid, the silver complex was found to have the most potent antioxidant and antidiabetic activities. The silver complex was the most potent, with an IC50 value that was higher than that of the standard drug. The studied compounds exhibited good physicochemical properties when compared with the standard reference drugs acarbose and ascorbic acid. The ADMET study examined the pharmacokinetics and toxicity of the free ligand and its Ag(I) complex, revealing the good drug-like behavior and nontoxic nature of these compounds.

AUTHOR CONTRIBUTIONS

Ceyhun Kucuk: Conceptualization; data curation; methodology; validation; software; writing—original draft. **Sibel Celik**: Conceptualization; data curation; methodology; software; supervision; validation; visualization; writing—original draft. **Senay Yurdakul**: Conceptualization; data curation; investigation; methodology; software; supervision; validation; visualization; writing—original draft. **Ebru Cotelı**: Writing—original draft.

CONFLICT OF INTEREST STATEMENT

There are no conflicts of interest to declare.

DATA AVAILABILITY STATEMENT

No data were used for the research described in the article.

REFERENCES

[1] G. Satija, B. Sharma, A. Madan, A. Iqubal, M. Shaquiquzzaman, M. Akhter, S. Parvez, M. A. Khan, M. M. Alam, *J. Heterocyclic Chem.* **2022**, *59*, 22.
[2] M. Gaba, S. Singh, C. Mohan, *Eur. J. Med. Chem.* **2014**, *76*, 494.
[3] M. Gaba, P. Gaba, D. Uppal, N. Dhingra, M. S. Bahiad, O. Silakari, C. Mohan, *Acta. Pharm. Sin. B.* **2015**, *5*(4), 337.
[4] S. Sharma, N. Anand, Benzimidazoles, in *Approaches to Design and Synthesis of Antiparasitic Drugs*, Pharmacochemistry Library, Elsevier **1997**.
[5] M. Correia, M. Rodrigues, P. Paiga, C. Delerue-Matos, Fungicides, in *Encyclopedia of Food and Health*, Academic Press, Cambridge, MA **2016**.
[6] K. C. S. Achar, K. M. Hosamani, H. R. Seetharamareddy, *Eur. J. Med. Chem.* **2010**, *45*(5), 2048.
[7] H. Iqbal, A. K. Verma, P. Yadav, S. Alam, M. Shafiq, D. Mishra, F. Khan, K. Hanif, A. S. Negi, D. Chanda, *Front. Pharmacol.* **2021**, *12*, 611109.
[8] X. J. Wang, M. Y. Xi, J. H. Fu, F. R. Zhang, G. F. Cheng, D. L. Yin, Q. D. You, *Chin. Chem. Lett.* **2012**, *23*, 707.
[9] J. Camacho, A. Barazarte, N. Gamboa, J. Rodrigues, R. Rojas, A. Vaisberg, R. Gilman, J. Charris, *Bioorg. Med. Chem.* **2023**, *2011*, 19.
[10] N. C. Desai, N. R. Shihory, G. M. Kotadiya, P. Desai, *Eur. J. Med. Chem.* **2014**, *82*, 480.
[11] A. M. Monforte, S. Ferro, L. D. Luca, G. L. Surdo, F. Morreale, C. Pannecouque, J. Balzarini, A. Chimirri, *Bioorg. Med. Chem.* **2014**, *22*, 1459.
[12] S. Tahlan, K. Ramasamy, S. M. Lim, S. A. A. Shah, V. Mani, B. Narasimhan, *BMC Chem.* **2019**, *3*(12), 1.
[13] M. Andrzejewskaa, L. Yepez-Mulia, A. Tapia, R. Cedillo-Rivera, A. E. Laudy, B. J. Starosciak, Z. Kazimierczuk, *Eur. J. Pharm. Sci.* **2004**, *21*, 323.
[14] K. Starcevic, M. Kralj, K. Ester, I. Sabol, M. Grce, K. Pavelic, G. Karminski-Zamolaa, *Bioorg. Med. Chem.* **2007**, *15*, 4419.
[15] H. Siddiquia, R. Farooq, B. P. Marasini, R. Malik, N. Syed, S. T. Moin, A. Rahman, M. I. Choudhary, *Bioorg. Med. Chem.* **2016**, *24*, 3387.

[16] S. Muthunatesan, V. Ragavendran, *Spectrochim. Acta A* **2015**, *134*, 148.
[17] D. Marcinkowski, M. W. Chorab, A. Bocian, J. Mikołajczyk, M. Kubicki, Z. Hnatejko, V. Patroniak, *Polyhedron* **2017**, *123*, 243.
[18] N. Sher, M. Ahmed, N. Mushtaq, R. A. Khan, *Appl. Organomet. Chem.* **2023**, *37*, e6950.
[19] H. O. Omoregie, T. L. Yusuf, S. D. Oladipo, K. A. Olofinsan, M. B. Kassim, S. Yousuf, *Polyhedron* **2022**, *217*, 115738.
[20] M. A. E. A. A. A. El-Remaily, O. Elhady, A. Abdou, D. Alhashmialameer, T. N. A. Eskander, *J. Mol. Struct.* **2023**, *1292*, 136188.
[21] H. M. A. El-Lateef, M. M. Khalaf, A. A. Amer, M. Kandeel, A. A. Abdelhamid, A. Abdou, *ACS Omega* **2023**, *29*, 25877.
[22] A. M. Najar, A. Eswayah, M. B. Moftah, O. M. K. Ruwida, E. Bobtaina, M. Najwa, T. A. Elhisadi, A. Tahani, S. M. Tawati, A. M. M. Khalifa, A. Abdou, A. E. DowAltome, *J. Med. Chem. Sci.* **2023**, *6*, 256.
[23] D. S. Badiger, R. S. Hunoor, B. R. Patil, R. S. Vadavi, C. V. Mangannavar, I. S. Muchchandi, Y. P. Patil, M. Nethaji, K. B. Gudasi, *Inorg. Chim. Acta* **2012**, *384*, 197.
[24] B. Iftikhar, K. Javed, M. S. U. Khan, Z. Akhter, B. Mirza, V. Mckee, *J. Mol. Struct.* **2018**, *1155*, 337.
[25] O. A. Abbas, O. M. El-Roudi, S. A. Abdel-Latif, *Appl. Organomet. Chem.* **2023**, *37*, e7236.
[26] A. E. M. Abdallah, S. A. Abdel-Latif, G. H. Elgemeie, *ACS Omega* **2023**, *8*, 19587.
[27] N. S. Abdel-Kader, S. A. Abdel-Latif, A. L. El-Ansary, M. A. Hemeda, *Polycyclic Aromat. Compd.* **2023**, 1.
[28] T. Murugan, R. Venkatesh, K. Geetha, A. Abdou, *Asian J. Chem.* **2023**, *35*(6), 1509.
[29] N. Ling, X. Wang, D. Zeng, Y. W. Zhang, X. Fang, H. X. Yang, *J. Mol. Struct.* **2020**, *1206*, 127641.
[30] E. J. Prpa, B. H. Bajka, P. R. Ellis, P. J. Butterworth, C. P. Corpe, W. L. Hall, *Crit. Rev. Food Sci. Nutr.* **2021**, *61*(22), 3783.
[31] S. Shahraki, M. H. Majd, A. Heydari, *J. Mol. Struct.* **2019**, *1177*, 536.
[32] M. N. A. Azeem, O. M. Ahmed, M. Shaban, K. N. M. Elsayed, *Sci. Pollut.* **2022**, *29*, 59930.
[33] H. A. S. Al-Shamiri, M. E. M. Sakr, S. A. Abdel-Latif, N. A. Negm, M. T. H. Abou Kana, S. A. El-Daly, A. H. M. Elwahy, *Sci. Rep.* **2022**, *12*, 19937.
[34] S. Shaaban, Y. S. Al-Faiyz, G. M. Alsulaim, M. Alaasar, N. Amri, H. Ba-Ghazal, A. A. Al-Karmalawy, A. Abdou, *Inorganics* **2023**, *11*, 321.
[35] N. Sher, M. Ahmed, N. Mushtaq, R. A. Khan, *Appl. Organomet. Chem.* **2022**, *3*, e6724.
[36] M. J. Frisch, G. W. Trucks, H. B. Schlegel, G. E. Scuseria, M. A. Robb, J. R. Cheeseman, G. Scalmani, V. Barone, B. Mennucci, G. A. Petersson, H. Nakatsuji, M. Caricato, X. Li, H. P. Hratchian, A. F. Izmaylov, J. Bloino, G. Zheng, J.L. Sonnenberg, M. Hada, M. Ehara, K. Toyota, R. Fukuda, J. Hasegawa, M. Ishida, T. Nakajima, Y. Honda, O. Kitao, H. Nakai, T. Vreven, J. A. Montgomery, J. E. Jr. Peralta, F. Ogliaro, M. Bearpark, J.J. Heyd, E. Brothers, K. N. Kudin, V. N. Staroverov, R. Kobayashi, J. Normand, K. Raghavachari, A. Rendell, J. C. Burant, S. S. Iyengar, J. Tomasi, M. Cossi, N. Rega, J. M. Millam, M. Klene, J. E. Knox, J. B. Cross, V. Bakken, C. Adamo, J. Jaramillo, R. Gomperts, R. E. Stratmann, O. Yazyev, A. J. Austin, R. Cammi, C. Pomelli, J. W. Ochterski, R. L. Martin, K. Morokuma, V. G. Zakrzewski, G. A. Voth, P. Salvador, J. J. Dannenberg, S. Dapprich, A. D. Daniels, O. Farkas, J. B. Foresman, J. V. Ortiz, J. Cioslowski, D. J. Fox, Gaussian, Inc., Wallingford CT, **2009**.
[37] R. Dennington, T. Keith, J. Millam, *GaussView, Version 5*, Semichem Inc., Shawnee Mission KS **2009**.
[38] A. D. Becke, *J. Chem. Phys.* **1993**, *98*, 5648.
[39] C. Lee, W. Yang, R. G. Parr, *Phys. Rev. E (3)* **1988**, *B37*, 785.
[40] J. J. Kores, I. A. Danish, T. Sasitha, J. G. Stuart, E. J. Pushpam, J. W. Jebaraj, *Heliyon* **2021**, *7*, e08377.
[41] N. S. Abdel-Kader, H. Moustafa, A. L. El-Ansaray, O. E. Sherif, A. M. Farghaly, *New. J. Chems.* **2021**, *45*, 7714.
[42] M. H. Jamroz, *Specrochim. Acta A* **2004**, *114*, 220.
[43] T. Lu, F. Chen, *J. Comput. Chem.* **2012**, *33*(5), 580.
[44] K. Subashini, S. Periandy, *J. Mol. Struct.* **2016**, *1117*, 240.
[45] A. Sadlej, J. Jaźwiński, *Chirality* **2021**, *33*, 660.
[46] G. M. Morris, D. S. Goodwill, R. S. Halliday, R. Huey, W. Hart, R. K. Belew, A. J. Olson, *J. Comput. Chem.* **1998**, *19*, 1639.
[47] RSCB PDB Protein Data Bank. https://www.rcsb.org/. Accessed 01 January 2024.
[48] Swiss Institute of Bioinformatics. www.swissadme.ch/index.php. Accessed 01 January 2024.
[49] PreADMET Citation Statistics. www.preadmet.com. Accessed 01 January 2024.
[50] ProTox-II- Prediction of Toxicity of Chemicals. http://tox.charite.de/protox_II/. Accessed 01 January 2024.
[51] E. Apostolidis, Y. I. Kwon, K. Shetty, *IFSET* **2007**, *8*, 46.
[52] M. S. Blois, *Nature* **1958**, *181*, 1199.
[53] L. Packer, M. Hiramatsu, T. Yoshikawa, *Antioxidant Food Supplements in Human Health*, Elsevier Inc. **1999**.
[54] K. Pannerselvan, M. S. García, *Acta Cryst. Sect. A* **1996**, *C52*, 1799.
[55] L. Ma, Y. H. Huang, J.-F. Xu, H. Deng, *Acta Cryst. Sect. A* **2011**, *E67*, 494.
[56] M. Govindarajan, K. Ganasan, S. Periandy, M. Karabacak, S. Mohan, *Spectrochim. Acta A* **2010**, *77*, 1005.
[57] S. Yurdakul, E. Temel, O. Büyükgüngör, *J. Mol. Struct.* **2019**, *1191*, 3001.
[58] R. Premkuma, R. M. Asath, T. Mathavan, A. M. F. Benial, *AIP Publ.* **2016**, *140041*, 1.
[59] [59]N. Sundaraganesan, S. Ilakiamani, P. Subramani, B. D. Joshua, *Spectrochim. Acta A* **2007**, *67*(3–4), 628.
[60] N. R. Babu, S. Subashchandrabose, M. S. A. Padusha, H. Saleem, V. MAnivannan, Y. Erdoğdu, *J. Mol. Struct.* **2014**, *25*(1072), 84.
[61] L. Vrielynck, J. P. Cornard, J. C. Merlin, M. F. Lautic, *Spectrochim. Acta A* **1994**, *50*, 2177.
[62] S. Murugavel, V. V. Velan, D. Kannan, M. Bakthadoss, *J. Mol. Struct.* **2016**, *1108*, 150.
[63] S. Celik, M. Alp, S. Yurdakul, *Spect. Lett.* **2020**, *53*(4), 234.
[64] A. Srivastava, R. Mishra, S. Kumar, K. Dev, P. Tandon, R. Maurya, *J. Mol. Struct.* **2015**, *1084*, 55.
[65] C. Kucuk, S. Celik, S. Yurdakul, E. Coteli, B. Erdem, *Polyhedron* **2023**, *241*, 116469.
[66] V. T. Nguyen, T. K. C. Huynh, G. T. T. Ho, T. H. A. Nguyen, T. L. A. Nguyen, D. Q. Dao, T. V. T. Mai, L. K. Huynh, T. K. D. Hoang, R. Soc, *Open Sci.* **2022**, *9*, 220659.

[67] M. T. Bilkan, S. Yurdakul, Z. Demircioglu, O. Büyükgüngor, *J. Organomet. Chem.* **2016**, *805*, 108.
[68] M. T. Bilkan, Ş. Yurdakul, *Russ. J. Inorg. Chem.* **2017**, *62*(7), 910.
[69] C. Kucuk, S. Yurdakul, S. Celik, B. Erdem, *Inorg. Chem. Commun.* **2022**, *145*, 109935.
[70] H. Kargar, M. F. Mehrjardi, R. B. Ardakani, K. S. Munawar, *J. Mol. Struct.* **2021**, *1245*, 131259.
[71] M. H. Rahuman, S. Muthu, B. R. Raajaraman, M. Raja, H. Umamahesvari, *Heliyon* **2020**, *6*(9), e04976.
[72] S. K. Alghamdi, F. Abbas, R. K. Hüseyin, A. G. Elhamzani, N. T. El-Shamy, *J. Mol. Struct.* **2023**, *1271*, 134001.
[73] T. Tsuneda, J. W. Song, S. Suzuki, K. Hirao, *J. Chem. Phys.* **2010**, *133*(17), 174101.
[74] Y. S. Mary, C. Y. Panicker, M. Sapnakumari, B. Narayana, B. K. Sarojini, A. A. Al Saadi, C. Vanalsenoy, J. A. War, *Spectrochim. Acta. A* **2015**, *136*, 483.
[75] D. Chen, H. Wang, *Proc. Combust. Inst.* **2019**, *37*, 953.
[76] S. Sowrirajan, N. Elangovan, G. Ajithkumar, K. P. Manoj, *Polycyclic Aromat. Compd.* **2022**, *42*(10), 7616.
[77] F. Boursas, F. Berrah, N. Kanagathara, G. Anbalagan, S. Bouacida, *J. Mol. Struct.* **2019**, *1180*, 532.
[78] N. Sivaskumar, N. Kanagathara, M. K. Marchewka, M. Drozd, R. Jayavel, G. Anbalagan, *Spectrochim. Acta A* **2018**, *204*, 717.
[79] P. Singh, S. S. Islam, H. Ahmad, A. Prabaharan, *J. Mol. Struct.* **2018**, *1154*, 39.
[80] A. Atilgan, Ş. Yurdakul, Y. Erdoğdu, M. T. Güllüoğlu, *J. Mol. Struct.* **2018**, *1161*, 55.
[81] F. B. Rizwana, J. C. Prasanaa, S. Muthu, C. S. Abraham, *Comput. Biol. Chem.* **2019**, *78*, 9.
[82] B. R. Raajaraman, N. R. Sheela, S. Muthu, *Comput. Biol. Chem.* **2019**, *82*, 44.
[83] C. Morell, A. Grand, A. Toro-Labbe, *J. Phys. Chem. A* **2005**, *109*, 205.
[84] B. Q. Sheeba, M. S. M. Mary, M. Amalanathan, C. B. Job, *Mol. Simul.* **2021**, *47*(15), 1217.
[85] M. Kim, E. Kim, H. S. Kwak, Y. Jeong, *Nutr. Res. Pract.* **2014**, *8*, 602.
[86] Y. J. Shim, H. K. Doo, S. Y. Ahn, Y. S. Kim, J. K. Seong, I. S. Park, B. H. Min, *J. Ethnopharmacol.* **2003**, *85*(2–3), 283.
[87] S. R. M. Ibrahim, G. A. Mohamed, M. T. Khayat, S. Ahmed, H. Abo-Haded, K. Z. Alshali, *Rev. Bras. Farmacogn.* **2019**, *2*, 206.
[88] X. Wang, N. Ling, Q. T. Che, Y. W. Zhang, H. X. Yang, Y. Ruan, T. T. Zhao, *Inor. Chem. Comm.* **2019**, *105*, 97.
[89] A. A. Akande, U. Salar, K. M. Khan, S. Syed, S. A. Aboaba, S. Chigurupati, A. Wadood, M. Riaz, M. Taha, S. Bhatia, K. S. Shamim, S. Perveen, *ACS Omega* **2021**, *6*(35), 22726.
[90] D. N. Patagar, S. R. Batakurki, R. Kusanur, S. M. Patraa, S. Saravanakumar, M. Ghatee, *J. Mol. Struct.* **2023**, *1274*, 134589.
[91] J. Deng, W. Cheng, G. Yang, *Food Chem.* **2011**, *125*(4), 1430.
[92] R. Scherer, H. T. Godoy, *Food Chem.* **2009**, *112*(3), 654.
[93] I. Sahin, M. Çesme, F. B. Ozgeris, F. Tümera, *Chem.-Biol. Interact.* **2023**, *370*, 110312.
[94] M. Kaur, R. Kaushal, *J. Mol. Struct.* **2023**, *1271*, 133994.
[95] G. A. Krishna, T. M. Dhanya, A. A. Shanty, K. G. Raghu, P. V. Mohanan, *J. Mol. Struct.* **2023**, *1274*, 134384.
[96] G. Maciejewska, W. Zierkiewicz, A. Adach, M. Kopacz, I. Zapała, I. Bulik, M. C. Golonka, T. Grabowski, J. Wietrzyk, *J. Inorg. Biochem.* **2009**, *103*, 1189.
[97] P. Padmaja, P. N. Reddy, B. V. S. Reddy, A. K. Tiwari, V. G. Ugale, A. Komati, B. Sridhar, *J. Mol. Struct.* **2023**, *1273*, 134238.
[98] M. D. Doan, S. L. Wang, V. B. Nguyen, T. K. P. Phan, Q. Phan, T. T. Nguyen, T. H. Nguyen, Q. V. Nguyen, A. D. Nguyen, *Res. Chem. Intermed.* **2023**, *49*, 5567.
[99] A. Khaldan, S. Bouamrane, R. El-mernissi, H. Maghat, M. A. Ajana, A. Sbai, M. Bouachrine, T. Lakhlifi, *Mater. Today: Proc.* **2021**, *45*(8), 7643.

SUPPORTING INFORMATION

Additional supporting information can be found online in the Supporting Information section at the end of this article.

How to cite this article: C. Kucuk, S. Celik, S. Yurdakul, E. Coteli, *Appl Organomet Chem* **2024**, *38*(6), e7499. https://doi.org/10.1002/aoc.7499